ISA Transactions 123 (2022) 46–60

Contents lists available at ScienceDirect

ISA Transactions

journal homepage: www.elsevier.com/locate/isatrans

Research article

Adaptive nonsingular fixed-time sliding mode control for uncertain robotic manipulators under actuator saturation ☆

Huayang Sai [a,b], Zhenbang Xu [a,c,*], Shuai He [a], Enyang Zhang [a], Lin Zhu [a,b,d]

[a] CAS Key Laboratory of On-orbit Manufacturing and Integration for Space Optics System, Changchun Institute of Optics, Fine Mechanics and Physics, Chinese Academy of Sciences, Changchun 130033, China
[b] University of Chinese Academy of Sciences, Beijing 100049, China
[c] Center of Materials Science and Optoelectronics Engineering, University of Chinese Academy of Sciences, Beijing 100049, China
[d] Institute of Applied Physics, Friedrich-Schiller-University Jena, Max-Wien-Platz 1, 07743 Jena, Germany

ARTICLE INFO

Article history:
Received 14 July 2020
Received in revised form 22 April 2021
Accepted 11 May 2021
Available online 25 May 2021

Keywords:
Fixed-time sliding mode control
Actuator saturation
Robotic manipulator
Uncertainties and disturbances

ABSTRACT

This paper describes an adaptive nonsingular fixed-time sliding mode control (ANFSMC) scheme under actuator saturation that can track the trajectory of a robotic manipulator under external disturbances and inertia uncertainties. First, a novel NFSMC that offers rapid convergence and avoids singularities is proposed for ensuring robotic manipulators global approximate fixed-time convergence. An ANFSMC is then developed for which the bound of the coupling uncertainty is not necessary to know in advance. The controller exhibits small absolute tracking errors and consumes little energy. An actuator saturation compensator is designed and shown to minimize the chattering of the system while accelerating the trajectory tracking. The proposed schemes are analyzed using Lyapunov stability theory, and their effectiveness and superiority are demonstrated through numerical simulations.

1. Introduction

With the further application of robots, increasingly onerous requirements are being placed on robot performance. However, due to external interference and the complex structure of the robotic manipulator, the precise control of robots remains a significant challenge [1]. Sliding mode control (SMC) has attracted wide attention due to its excellent robustness to uncertainties and disturbances and is widely used in the field of robots [2–5].

Although SMC has gained popularity, it still has some fatal flaws. Chattering is the main barrier to SMC application, as it seriously degrades the tracking performance of the controlled robotic manipulator system. Moreover, the conventional SMC motion to the origin is accomplished asymptotically, that is, the tracking error of the system converges to the origin over time. The finite-time control ensures fast and high-precision tracking performance for the control system. A terminal sliding mode control (TSMC) algorithm was designed to guarantee finite-time state convergence [6]. Feng et al. [7] proposed a nonsingular TSMC (NTSMC) to overcome the singularity in TSMC by designing an appropriate fractional power in the controller. To further accelerate the convergence of NTSMC, a fast NTSMC (FNTSMC) scheme was developed [8]. Compared with other sliding mode surfaces, FNTSMC can achieve finite-time state convergence and fast convergence when the state is far from the origin, which avoids the singularity problem and reduces the incidence of chattering. A novel FNTSMC manifold without any constraints was proposed to achieve finite-time tracking control for spacecraft attitude [9]. To avoid the computational burden of feedback linearization and complex inverse matrices, a novel nonsingular super-twisted integral SMC scheme was proposed for finite-time attitude stabilization control of rigid body subject with unknown disturbances [10]. However, the time required to establish finite-time SMC depends on the initial state of the system, making it difficult to calculate the establishment time of trajectory tracking ahead of time.

For the last few years, scholars have proposed the fixed-time control theory, which is a further development of conventional SMC methods. Fixed-time control can guarantee a bounded settling time and autonomy from the initial condition of the system, and it can provide faster transients and higher control accuracy than finite-time control [11]. Researchers have conducted detailed mathematical analyses of fixed-time stability and convergence [12–14]. A fixed-time control algorithm based on SMC has been proposed, with a new fixed-time manifold introduced to guarantee that the system has a fast merging speed [15].

☆ This work is partially supported by the National Natural Science Foundation of China (11972343, 91848202), the Funded and Supported by National Key R&D Program of China (No. 2016YFE0205000).

* Corresponding author at: CAS Key Laboratory of On-orbit Manufacturing and Integration for Space Optics System, Changchun Institute of Optics, Fine Mechanics and Physics, Chinese Academy of Sciences, Changchun 130033, China.
E-mail address: xuzhenbang@ciomp.ac.cn (Z. Xu).

https://doi.org/10.1016/j.isatra.2021.05.011
0019-0578/

Golestani et al. [16] proposed a novel nonsingular fast fixed-time SMC algorithm for spacecrafts with system uncertainties. Li et al. [17] proposed a fixed-time SMC scheme for single inverted pendulum systems, while Zuo [18] designed a new sliding mode surface to avoid the singularity of fixed-time SMC. The above-mentioned studies indicate that most existing fixed-time controllers apply to linear and nonlinear affine systems, but they cannot be easily applied to uncertain robotic manipulators. To calculate the settling time of robotic manipulator trajectory tracking error, a novel fixed-time SMC was proposed, which can track the global fixed-time trajectory of the robotic manipulator with uncertain model dynamics and bounded disturbances [19]. Su et al. [20] proposed a global approximate fixed-time control method for manipulators in uncertain states, which enables the tracking errors to converge to an arbitrarily small range within a uniform predetermined time. However, the above-mentioned control schemes assume some forward knowledge regarding the upper bound of the coupling uncertainty, and it is not easily available in practical engineering.

In the existing literature, the problem of system and external disturbance uncertainties has been widely studied through the following three methods: (i) Intelligent algorithms such as neural networks (NNs) were used to approximate the system uncertainties. Several scholars have proposed using radial basis function NNs to estimate the nonlinear robotic manipulator dynamics and disturbances, thus improving the control effect of fixed-time SMC [21–23]. However, NNs are computationally intensive and struggle to achieve real-time control of robotic manipulators. (ii) Disturbance observers have been developed and used to predict the unknown external disturbance. Nevertheless, the position tracking performance of the robotic depends largely on the effect of the designed observer and the estimated noise of the disturbances is always large, thus requiring additional filters [24–26]. (iii) The adaptive control algorithm is a simple but effective method to adjust the controller to adapt to the coupling uncertainty of the system. For instance, an adaptive global fast TSMC was used for a MEMS gyro with model uncertainties and disturbance [27]. Besides, adaptive second-order TSMC and adaptive nonsingular fast TSMC (ANFTSMC) methods were developed for trajectory tracking of robotic manipulators with coupling uncertainty [28,29].

Since fixed-time control requires a fast instantaneous response, the actuator of the robotic manipulator is likely to be saturated due to large control torque. The uncertainty and saturation of the actuator are usually considered in the robust control of the spacecraft. For example, fixed-time attitude control frameworks are presented to separately spacecraft, and they can ensure fixed-time stability of the spacecraft system even in the case of saturation and faults of the actuator [30,31]. Novel observers were designed for spacecraft attitude tracking by taking the system uncertainties, actuator saturation, and finite-time issues into account [26,32]. It is noting that combining the input error caused by actuator saturation with system uncertainties and disturbances imposes a computational burden on the observer, and the dynamics of the system can be greatly affected by the additional disturbance caused by actuator saturation. A robust controller for manipulators with actuator faults was proposed in [33], and it has been applied to the control experiment of robotic. Jia et al. [34] proposed a novel auxiliary system for compensating the saturation of space manipulator actuators, but this still requires some prior knowledge of the system uncertainties.

As discussed above, few existing studies simultaneously consider the system uncertainties and disturbances in the context of fixed-time SMC, system singularities, and actuator saturation. Consequently, this paper describes three SMC schemes that are designed to overcome the above problems. These schemes are mainly based on nonsingular fixed-time SMC, an adaptive control law, and an actuator saturation compensator. The overall contribution of this study includes: (1) A novel nonsingular fixed-time SMC (NFSMC) scheme is designed. It is demonstrated that the tracking errors of manipulators can reach an arbitrary small domain near zero with a bounded time. (2) An adaptive parameter adjustment program is proposed in the estimation of the upper bound of the lumped uncertainty. Consequently, the bound of the lumped uncertainty need not be known or estimated. Moreover, the proposed adaptive nonsingular fixed-time SMC (ANFSMC) offers faster trajectory tracking and requires less energy than several previous control schemes [8,19,29]. (3) Considering actuator saturation, an actuator saturation compensator is designed for ANFSMC. The resulting ANFSMC-AS can adaptively compensate the control input when the actuator control torque is saturated. The compensated controller has a faster trajectory tracking rate with less joint chattering than before compensation.

The paper is organized as follows. Some symbol definitions and lemmas are introduced in Section 2. In Section 3, the NFSMC, ANFSMC, and ANFSMC-AS schemes are designed, and their stabilities are proved using Lyapunov stability theory. In Section 4, the proposed ANFSMC scheme is simulated in a two-link manipulator. The numerical simulation results are compared with those given by the control schemes in [8,19,29]. Finally, this work and future direction are summarized in Section 5.

2. Preliminaries and notation

2.1. Notions

For an n-dimensional vector $\boldsymbol{x} = [x_1, x_2, \dots, x_n]^T$, x_i $(i = 1, \dots, n)$ denotes the ith element of vector $\boldsymbol{x}$. The norm of matrix $\boldsymbol{A} \in R^{n\times n}$ and vector $\boldsymbol{x} \in R^n$ are defined as $\|\boldsymbol{A}\| = tr\left(\boldsymbol{A}^T\boldsymbol{A}\right)$ and $\|\boldsymbol{x}\| = \sqrt{\boldsymbol{x}^T\boldsymbol{x}}$. $\lambda_{\min}\{\boldsymbol{A}\}$ and $\lambda_{\max}\{\boldsymbol{A}\}$ denote the smallest and largest eigenvalues, respectively. $\operatorname{sign}(x)$ denotes the signum function, and the nonlinear function $\operatorname{sig}^\alpha(x)$ and vector $\mathbf{Sig}^\alpha(\boldsymbol{x}) \in R^n$ are defined as

$$\operatorname{sig}^\alpha(x) = |x|^\alpha \operatorname{sign}(x), \ (\alpha > 0) \tag{1}$$

$$\mathbf{Sig}^\alpha(\boldsymbol{x}) = \left[|x_1|^\alpha \operatorname{sign}(x_1), \dots, |x_n|^\alpha \operatorname{sign}(x_n)\right]^T. \ (\alpha > 0) \tag{2}$$

The saturation function can be denoted as

$$\operatorname{sat}(x) = \begin{cases} \operatorname{sign}(x)\, x_{\max}, & |x| \geqslant x_{\max} \\ x, & |x| < x_{\max}. \end{cases} \tag{3}$$

2.2. Some definitions and lemmas

Consider the following nonlinear system

$$\dot{\boldsymbol{x}} = f(\boldsymbol{x}; \boldsymbol{\rho}), \ \boldsymbol{x}(0) = \boldsymbol{x}_0, \tag{4}$$

where $\boldsymbol{x} \in R^n$ is the system state, and the vector $\boldsymbol{\rho} \in R^n$ denotes the system parameters. The function $f : U_0 \to R^n$ is a continuous function in an open neighborhood U_0 of the origin, and $f(0) = 0$.

Definition 1 (*Finite-Time Stability [35,36]*)**.** The control system (4) is called globally finite-time stable if it is globally asymptotically stable, and for any $\boldsymbol{x}_0 \in R^n$ there exists a time moment $T(x_0)$ satisfies the solution $\boldsymbol{x}(t, \boldsymbol{x}_0) = 0$ for all $t \geqslant T$.

Definition 2 (*Fixed-Time Stability [11]*)**.** The control system (4) is called globally fixed-time stable if it is globally finite-time stable and there is a time T such that the system state converges to zero, i.e. $\boldsymbol{x}(t, \boldsymbol{x}_0) = 0$ for all $t \geqslant T$.

Lemma 1 ([37]). *For the following scalar system*

$$\dot{y} = -\epsilon_1 y^{\frac{m}{n}} - \epsilon_2 y^{\frac{p}{q}}, y(0) = y_0, \tag{5}$$

where $\epsilon_1 > 0, \epsilon_2 > 0$, and m, n, p, q are all positive odd integers that satisfy $m > n, p < q$, system (5) is globally fixed-time stable with the guaranteed convergence time T bounded by

$$T < T_{\max} \triangleq \frac{1}{\epsilon_1}\frac{n}{m-n} + \frac{1}{\epsilon_2}\frac{q}{q-p}. \tag{6}$$

Lemma 2 ([38]). *Consider $\xi_1, \xi_2, \ldots, \xi_N \geqslant 0$. Then,*

$$\sum_{i=1}^{N} \xi_i^p \geq \left(\sum_{i=1}^{N} \xi_i\right)^p \quad \text{if } 0 < p \leq 1 \tag{7}$$

$$\sum_{i=1}^{N} \xi_i^p \geq N^{1-p} \left(\sum_{i=1}^{N} \xi_i\right)^p \quad \text{if } 1 < p < \infty. \tag{8}$$

Lemma 3. *With a positive constant α and a variable $x \in R^n$, they satisfy the following inequality*

$$d\,|x|^{\alpha+1}/dx = (\alpha+1)\,|x|^{\alpha}\,\mathrm{sign}(x) \tag{9}$$

$$d\left[|x|^{\alpha+1}\,\mathrm{sign}(x)\right]/dx = (\alpha+1)\,|x|^{\alpha}. \tag{10}$$

2.3. Dynamic model of robots

Consider the following Cartesian dynamics of a general n-degrees-of-freedom (DOF) rigid robotic manipulator system

$$\boldsymbol{M}(\boldsymbol{q})\ddot{\boldsymbol{q}} + \boldsymbol{C}(\boldsymbol{q},\dot{\boldsymbol{q}})\dot{\boldsymbol{q}} + \boldsymbol{G}(\boldsymbol{q}) = \boldsymbol{\tau} + \boldsymbol{\tau_d}, \tag{11}$$

where $\boldsymbol{q}, \dot{\boldsymbol{q}}, \ddot{\boldsymbol{q}} \in R^n$ are the position, velocity, and acceleration vector of the robotic manipulator. $\boldsymbol{M}(\boldsymbol{q}) \in R^{n\times n}$ denotes the inertia matrix, and $\boldsymbol{C}(\boldsymbol{q},\dot{\boldsymbol{q}}) \in R^{n\times n}$ denotes the centrifugal-Coriolis matrix. $\boldsymbol{G}(\boldsymbol{q}) \in R^n$ is the vector of Cartesian gravitational forces. $\boldsymbol{\tau}$ denotes the vector of joint torque inputs, and $\boldsymbol{\tau_d}$ is a vector of bounded but unknown disturbances.

Property 1 ([39]). *Generally, $\boldsymbol{M}(\boldsymbol{q})$, $\boldsymbol{C}(\boldsymbol{q},\dot{\boldsymbol{q}})$, and $\boldsymbol{G}(\boldsymbol{q})$ are always unknown, and they can be written as*

$$\begin{cases} \boldsymbol{M}(\boldsymbol{q}) = \boldsymbol{M}_0(\boldsymbol{q}) + \Delta\boldsymbol{M}(\boldsymbol{q}) \\ \boldsymbol{C}(\boldsymbol{q},\dot{\boldsymbol{q}}) = \boldsymbol{C}_0(\boldsymbol{q},\dot{\boldsymbol{q}}) + \Delta\boldsymbol{C}(\boldsymbol{q},\dot{\boldsymbol{q}}) \\ \boldsymbol{G}(\boldsymbol{q}) = \boldsymbol{G}_0(\boldsymbol{q}) + \Delta\boldsymbol{G}(\boldsymbol{q}) \end{cases} \tag{12}$$

where $\boldsymbol{M_0}(\boldsymbol{q})$, $\boldsymbol{C_0}(\boldsymbol{q},\dot{\boldsymbol{q}})$, and $\boldsymbol{G_0}(\boldsymbol{q})$ are the nominal values, and $\Delta\boldsymbol{M}(\boldsymbol{q})$, $\Delta\boldsymbol{C}(\boldsymbol{q},\dot{\boldsymbol{q}})$, $\Delta\boldsymbol{G}(\boldsymbol{q})$ represent the system uncertainties.

Property 2 ([39]). *$\boldsymbol{M}(\boldsymbol{q})$, $\boldsymbol{C}(\boldsymbol{q},\dot{\boldsymbol{q}})$, and $\boldsymbol{G}(\boldsymbol{q})$ are all bounded matrices, and $\boldsymbol{M}(\boldsymbol{q})$ satisfies*

$$M_m \leqslant \|\boldsymbol{M}(\boldsymbol{q})\| \leqslant M_M, \text{for } \forall \boldsymbol{q} \in R^n \tag{13}$$

where M_m, M_M are both known positive constants.

Then, the dynamic equation given by Eq. (11) can lead to

$$\boldsymbol{M_0}(\boldsymbol{q})\ddot{\boldsymbol{q}} + \boldsymbol{C_0}(\boldsymbol{q},\dot{\boldsymbol{q}})\dot{\boldsymbol{q}} + \boldsymbol{G_0}(\boldsymbol{q}) = \boldsymbol{\tau} + \boldsymbol{F_d}(\boldsymbol{q},\dot{\boldsymbol{q}},\ddot{\boldsymbol{q}}), \tag{14}$$

where the lumped uncertainty $\boldsymbol{F_d}(\boldsymbol{q}, \dot{\boldsymbol{q}}, \ddot{\boldsymbol{q}})$ is defined as

$$\boldsymbol{F_d}(\boldsymbol{q},\dot{\boldsymbol{q}},\ddot{\boldsymbol{q}}) = \boldsymbol{\tau_d} - \Delta\boldsymbol{M}(\boldsymbol{q})\ddot{\boldsymbol{q}} - \Delta\boldsymbol{C}(\boldsymbol{q},\dot{\boldsymbol{q}})\dot{\boldsymbol{q}} - \Delta\boldsymbol{G}(\boldsymbol{q}). \tag{15}$$

The position tracking error, speed tracking error and acceleration error are denoted as

$$\boldsymbol{e} = \boldsymbol{q} - \boldsymbol{q_d}, \ \dot{\boldsymbol{e}} = \dot{\boldsymbol{q}} - \dot{\boldsymbol{q}}_{\boldsymbol{d}}, \ \ddot{\boldsymbol{e}} = \ddot{\boldsymbol{q}} - \ddot{\boldsymbol{q}}_{\boldsymbol{d}}. \tag{16}$$

3. Control development

In this section, an NFSMC algorithm for the tracking control of rigid manipulators is proposed. The main advantages of this NFSMC algorithm are its fast convergence, singularity-free, and convergence time independent of the initial states of the system. Generally, the bound of the coupling uncertainty $\boldsymbol{F_d}$ is not easily obtained in practical applications (for simplification, $\boldsymbol{F_d}(\boldsymbol{q}, \dot{\boldsymbol{q}}, \ddot{\boldsymbol{q}})$ is written as $\boldsymbol{F_d}$ in the remainder of this paper); thus the AN-FSMC is designed to compensate the model uncertainties and disturbances. Considering that actuator saturation may occur in the robotic manipulator because the fixed-time control requires a large control torque to guarantee a rapid transient response, a saturation compensator is developed to compensate for system inputs.

3.1. Design approach for NFSMC

A nonlinear function $f(x)$ is proposed as [19]:

$$f(x) = \begin{cases} k_1 \mathrm{sig}^r(x) + k_2 \delta^{|x|} x \ \text{if } |x| < \delta \\ \mathrm{sig}^{\alpha}(x) \ \ \text{if } |x| \geqslant \delta \end{cases} \tag{17}$$

where $\delta \in (0, \exp(-1)), r = 2 - \delta, \alpha = 1 - \delta$. The constants k_1 and k_2 are defined as

$$k_1 = \frac{-1 - \ln\delta}{\alpha - \delta\ln\delta}, k_2 = \frac{\delta^{2\alpha-2}}{\alpha - \delta\ln\delta}. \tag{18}$$

Considering the Lemma 3, the time derivative of $f(x)$ is calculated by

$$\dot{f}(x) = \begin{cases} k_1 r\,|x|^{r-1} + k_2(|x|\ln\delta + 1)\,\delta^{|x|} \ \text{if } |x| < \delta \\ \alpha\,|x|^{\alpha-1} \ \ \text{if } |x| \geqslant \delta. \end{cases} \tag{19}$$

Then, define the vector $\boldsymbol{F}(\boldsymbol{x})$ and the diagonal matrix $\dot{\boldsymbol{F}}(\boldsymbol{x})$ as

$$\boldsymbol{F}(\boldsymbol{x}) = [f(x_1), f(x_2), \ldots, f(x_n)]^T, \tag{20}$$

$$\dot{\boldsymbol{F}}(\boldsymbol{x}) = \mathrm{diag}\left\{\dot{f}(x_i)\right\}, i = 1, 2, \ldots, n. \tag{21}$$

An NFSMC surface $\boldsymbol{s}$ is introduced as [19]:

$$\boldsymbol{s} = \dot{\boldsymbol{e}} + \boldsymbol{C}_1\boldsymbol{F}(\boldsymbol{e}) + \boldsymbol{C}_2\mathbf{Sig}^{\beta}(\boldsymbol{e}), \tag{22}$$

where $\boldsymbol{C}_1, \boldsymbol{C}_2$ are two positive-definite diagonal matrixes, and $\beta > 1$ is a defined positive constant. Thus,

$$\dot{\boldsymbol{s}} = \ddot{\boldsymbol{e}} + \boldsymbol{C}_1\dot{\boldsymbol{F}}(\boldsymbol{e}) + \boldsymbol{C}_2\boldsymbol{D}^{\beta-1}(\boldsymbol{e})\,\dot{\boldsymbol{e}}, \tag{23}$$

where the diagonal matrix $\boldsymbol{D}^r(\boldsymbol{\xi}) \in R^{n\times n}$ is defined as

$$\boldsymbol{D}^r(\boldsymbol{\xi}) = \mathrm{diag}\left\{|\xi_i|^r\right\}, i = 1, 2, \ldots, n. \tag{24}$$

The overall NFSMCer can be designed as

$$\boldsymbol{\tau} = -\boldsymbol{\tau}_0 + \boldsymbol{\tau}_1 + \boldsymbol{\tau}_2 \tag{25}$$

$$\begin{aligned} \boldsymbol{\tau}_0 = {} & \boldsymbol{C}_1\boldsymbol{M}_0(\boldsymbol{q})\dot{\boldsymbol{F}}(\boldsymbol{e})\dot{\boldsymbol{e}} + \boldsymbol{C}_2\boldsymbol{M}_0(\boldsymbol{q})\boldsymbol{D}^{\beta-1}(\boldsymbol{e})\dot{\boldsymbol{e}} \\ & - \boldsymbol{C}_0(\boldsymbol{q},\dot{\boldsymbol{q}})\dot{\boldsymbol{q}} - \boldsymbol{G}_0(\boldsymbol{q}) - \boldsymbol{M}_0(\boldsymbol{q})\ddot{\boldsymbol{q}}_{\boldsymbol{d}} \end{aligned} \tag{26}$$

$$\boldsymbol{\tau}_1 = -\boldsymbol{K_p}\mathbf{Sig}^{\upsilon_1}(\boldsymbol{s}) - \boldsymbol{K_d}\mathbf{Sig}^{\upsilon_2}(\boldsymbol{s}) \tag{27}$$

$$\boldsymbol{\tau}_2 = -\mathrm{sign}(\boldsymbol{s})\,\eta, \tag{28}$$

where $\upsilon_1 > 1$ and $0 < \upsilon_2 < 1$ are positive constants and $\boldsymbol{K_p}, \boldsymbol{K_d} \in R^{n\times n}$ are positive-definite diagonal matrixes. $\dot{\boldsymbol{F}}(\boldsymbol{e})$ and β are defined by Eqs. (21) and (22), respectively. The nominal part $\eta \in R^n$ is

$$\eta = \frac{1}{1-\sigma}\exp\left(\left\|\boldsymbol{M}_0^{-1}(\boldsymbol{q})\right\|^{\varepsilon} - 1\right)$$

$$\times\ \left(b_0 + b_1 \|\boldsymbol{q}\| + b_2 \|\dot{\boldsymbol{q}}\|^2 + \sigma \|\boldsymbol{\tau}_1 - \boldsymbol{\tau}_0\|\right), \tag{29}$$

$$\varepsilon = \varepsilon_0 \operatorname{sign}\left(\left\|\boldsymbol{M}_0^{-1}(\boldsymbol{q})\right\| - 1\right), \tag{30}$$

$$\sigma = \frac{m_2 - m_1}{m_1 + m_2}, \tag{31}$$

where ε_0 is a known positive constant, and b_0, b_1, b_2 are three positive constants. m_1 and m_2 are two positive constants satisfy $m_1 \leqslant \left\|\boldsymbol{M}^{-1}(\boldsymbol{q})\right\| \leqslant m_2$.

Property 3 ([40,41]). *The coupling uncertainty $\boldsymbol{F_d}$ is bounded by*

$$\|\boldsymbol{F_d}\| < b_0 + b_1 \|\boldsymbol{q}\| + b_2 \|\dot{\boldsymbol{q}}\|^2 + \sigma \|\boldsymbol{\tau}\|, \tag{32}$$

where b_0, b_1, b_2 and σ are known positive constants, and defined by Eqs. (29) and (31), and the relevant proof can be found in [40,41].

Theorem 1. *For the control scheme in Eqs. (25)–(28), the tracking error can converge inside some fixed time T, and the settling time T includes the reaching time T_r and the sliding time T_s. The reaching time T_r represents the period in which the tracking trajectory converges to the sliding surface $s = 0$, and the sliding time T_s represents the period in which the tracking error along the sliding mode surface reaches an arbitrarily small domain of the origin. T, T_r, T_s can be written in the following inequalities:*

$$T < T_{\max} \triangleq T_r + T_s, \tag{33}$$

$$T_r \leqslant \frac{2(m_1+m_2)^{-(1+v_1)/2}}{\lambda_{\min}\left\{\boldsymbol{K_p}\right\} n^{(1-v_1)/2}(v_1 - 1)} + \frac{2(m_1+m_2)^{-(1+v_2)/2}}{\lambda_{\min}\left\{\boldsymbol{K_d}\right\}(1 - v_2)}, \tag{34}$$

$$T_s \leqslant \frac{2^{\frac{1-\alpha}{2}}}{(1-\alpha)\lambda_{\min}(\boldsymbol{C}_1)} + \frac{\left(\frac{2}{n}\right)^{\frac{1-\beta}{2}}}{(\beta - 1)\lambda_{\min}(\boldsymbol{C}_2)}. \tag{35}$$

Proof. The stability analysis of the proposed NFSMC scheme includes the reaching phase and the sliding phase.

Step 1. Stability and settling time analysis in reaching phase: By multiplying both sides of Eq. (23) by $\boldsymbol{M}_0(\boldsymbol{q})$, we have

$$\boldsymbol{M}_0(\boldsymbol{q})\dot{\boldsymbol{s}} = \boldsymbol{M}_0(\boldsymbol{q})\ddot{\boldsymbol{e}} + \boldsymbol{C}_1\boldsymbol{M}_0(\boldsymbol{q})\dot{\boldsymbol{F}}(\boldsymbol{e})\dot{\boldsymbol{e}} + \boldsymbol{C}_2\boldsymbol{M}_0(\boldsymbol{q})\boldsymbol{D}^{\beta-1}(\boldsymbol{e})\dot{\boldsymbol{e}}. \tag{36}$$

Substituting Eqs. (15), (16) and (26) into Eq. (36) yields

$$\begin{aligned}\boldsymbol{M}_0(\boldsymbol{q})\dot{\boldsymbol{s}} &= \boldsymbol{M}_0(\boldsymbol{q})\ddot{\boldsymbol{q}} - \boldsymbol{M}_0(\boldsymbol{q})\ddot{\boldsymbol{q}}_{\boldsymbol{d}} + \boldsymbol{\tau}_0 \\ &\quad + \boldsymbol{C}_0(\boldsymbol{q},\dot{\boldsymbol{q}})\dot{\boldsymbol{q}} + \boldsymbol{G}_0(\boldsymbol{q}) + \boldsymbol{M}_0(\boldsymbol{q})\ddot{\boldsymbol{q}}_{\boldsymbol{d}} \\ &= \boldsymbol{\tau}_1 + \boldsymbol{\tau}_2 + \boldsymbol{F_d}.\end{aligned} \tag{37}$$

Consider the Lyapunov function as

$$V_1 = \frac{1}{2}\boldsymbol{s}^T\boldsymbol{M}_0\boldsymbol{s}. \tag{38}$$

Taking the derivative V_1 with regard to time yields

$$\begin{aligned}\dot{V}_1 &= \boldsymbol{s}^T\boldsymbol{M}_0\dot{\boldsymbol{s}} = \boldsymbol{s}^T(\boldsymbol{\tau}_1 + \boldsymbol{\tau}_2 + \boldsymbol{F_d}) \\ &= -\boldsymbol{s}^T\left(\boldsymbol{K_p}\mathbf{Sig}^{v_1}(\boldsymbol{s}) + \boldsymbol{K_d}\mathbf{Sig}^{v_2}(\boldsymbol{s})\right) - \|\boldsymbol{s}\|\eta + \boldsymbol{s}^T\boldsymbol{F_d} \\ &\leqslant -\boldsymbol{s}^T\left(\boldsymbol{K_p}\mathbf{Sig}^{v_1}(\boldsymbol{s}) + \boldsymbol{K_d}\mathbf{Sig}^{v_2}(\boldsymbol{s})\right) - \|\boldsymbol{s}\|\eta + \|\boldsymbol{s}\|\|\boldsymbol{F_d}\|.\end{aligned} \tag{39}$$

Considering Eq. (32), $\dot{V}_1$ can be written as

$$\begin{aligned}\dot{V}_1 \leqslant &-\|\boldsymbol{s}\|\eta + \left(b_0 + b_1\|\boldsymbol{q}\| + b_2\|\dot{\boldsymbol{q}}\|^2 + \sigma\|\boldsymbol{\tau}\|\right)\|\boldsymbol{s}\| \\ &- \boldsymbol{s}^T\left(\boldsymbol{K_p}\mathbf{Sig}^{v_1}(\boldsymbol{s}) + \boldsymbol{K_d}\mathbf{Sig}^{v_2}(\boldsymbol{s})\right).\end{aligned} \tag{40}$$

From Eq. (25), it is easy to obtain

$$\|\boldsymbol{\tau}\| \leqslant \|\boldsymbol{\tau}_1 - \boldsymbol{\tau}_0\| + \|\boldsymbol{\tau}_2\|. \tag{41}$$

Then, Eq. (40) can be written as

$$\begin{aligned}\dot{V}_1 &\leqslant -\|\boldsymbol{s}\|\eta + \left(b_0 + b_1\|\boldsymbol{q}\| + b_2\|\dot{\boldsymbol{q}}\|^2 + \sigma\|\boldsymbol{\tau}_1 - \boldsymbol{\tau}_0\|\right)\|\boldsymbol{s}\| \\ &\quad + \sigma\|\boldsymbol{\tau}_2\|\|\boldsymbol{s}\| - \boldsymbol{s}^T\left(\boldsymbol{K_p}\mathbf{Sig}^{v_1}(\boldsymbol{s}) + \boldsymbol{K_d}\mathbf{Sig}^{v_2}(\boldsymbol{s})\right) \\ &= -(1-\sigma)\|\boldsymbol{s}\|\eta - \sigma\|\boldsymbol{s}\|\eta + \sigma\|\boldsymbol{\tau}_2\|\|\boldsymbol{s}\| \\ &\quad + \left(b_0 + b_1\|\boldsymbol{q}\| + b_2\|\dot{\boldsymbol{q}}\|^2 + \sigma\|\boldsymbol{\tau}_1 - \boldsymbol{\tau}_0\|\right)\|\boldsymbol{s}\| \\ &\quad + \sigma\|\boldsymbol{\tau}_2\|\|\boldsymbol{s}\| - \boldsymbol{s}^T\left(\boldsymbol{K_p}\mathbf{Sig}^{v_1}(\boldsymbol{s}) + \boldsymbol{K_d}\mathbf{Sig}^{v_2}(\boldsymbol{s})\right) \\ &= \left(1 - \exp\left(\left\|\boldsymbol{M}_0^{-1}(\boldsymbol{q})\right\|^{\varepsilon} - 1\right)\right) \\ &\quad \times \left(b_0 + b_1\|\boldsymbol{q}\| + b_2\|\dot{\boldsymbol{q}}\|^2 + \sigma\|\boldsymbol{\tau}_1 - \boldsymbol{\tau}_0\|\right)\|\boldsymbol{s}\| \\ &\quad - \sigma\|\boldsymbol{s}\|\eta + \sigma\|\boldsymbol{\tau}_2\|\|\boldsymbol{s}\| - \boldsymbol{s}^T\left(\boldsymbol{K_p}\mathbf{Sig}^{v_1}(\boldsymbol{s}) + \boldsymbol{K_d}\mathbf{Sig}^{v_2}(\boldsymbol{s})\right).\end{aligned} \tag{42}$$

Considering Eq. (30), it is easy to see that $\left\|\boldsymbol{M}_0^{-1}(\boldsymbol{q})\right\|^{\varepsilon} \geqslant 1$, and then we can get $\exp\left(\left\|\boldsymbol{M}_0^{-1}(\boldsymbol{q})\right\|^{\varepsilon} - 1\right) \geqslant 1$. Eq. (42) can be bounded by

$$\begin{aligned}\dot{V}_1 &\leqslant -\sigma\|\boldsymbol{s}\|\eta + \sigma\|\boldsymbol{\tau}_2\|\|\boldsymbol{s}\| - \boldsymbol{s}^T\left(\boldsymbol{K_p}\mathbf{Sig}^{v_1}(\boldsymbol{s}) + \boldsymbol{K_d}\mathbf{Sig}^{v_2}(\boldsymbol{s})\right) \\ &= -\sigma\|\boldsymbol{s}\|\eta + \sigma\|\boldsymbol{s}\|\|\operatorname{sign}(\boldsymbol{s})\eta\| \\ &\quad - \boldsymbol{s}^T\left(\boldsymbol{K_p}\mathbf{Sig}^{v_1}(\boldsymbol{s}) + \boldsymbol{K_d}\mathbf{Sig}^{v_2}(\boldsymbol{s})\right) \\ &= -\boldsymbol{s}^T\left(\boldsymbol{K_p}\mathbf{Sig}^{v_1}(\boldsymbol{s}) + \boldsymbol{K_d}\mathbf{Sig}^{v_2}(\boldsymbol{s})\right).\end{aligned} \tag{43}$$

According to Lemma 2, we obtain

$$\begin{aligned}\boldsymbol{s}^T\boldsymbol{K_p}\mathbf{Sig}^{v_1}(\boldsymbol{s}) &= \sum_{i=1}^{n} k_{pi}|s_i|^{1+v_1} \geqslant \lambda_{\min}\left\{\boldsymbol{K_p}\right\}\sum_{i=1}^{n}|s_i|^{1+v_1} \\ &\geqslant \lambda_{\min}\left\{\boldsymbol{K_p}\right\} n^{\frac{1-v_1}{2}}\left(\sum_{i=1}^{n}|s_i|^2\right)^{\frac{1+v_1}{2}}\end{aligned} \tag{44}$$

$$\begin{aligned}\boldsymbol{s}^T\boldsymbol{K_d}\mathbf{Sig}^{v_1}(\boldsymbol{s}) &= \sum_{i=1}^{n} k_{di}|s_i|^{1+v_2} \geqslant \lambda_{\min}\left\{\boldsymbol{K_d}\right\}\sum_{i=1}^{n}|s_i|^{1+v_2} \\ &\geqslant \lambda_{\min}\left\{\boldsymbol{K_d}\right\}\left(\sum_{i=1}^{n}|s_i|^2\right)^{\frac{1+v_2}{2}}.\end{aligned} \tag{45}$$

Substituting Eqs. (44) and (45) into Eq. (43) yields

$$\begin{aligned}\dot{V}_1 \leqslant &-\lambda_{\min}\left\{\boldsymbol{K_p}\right\} n^{\frac{1-v_1}{2}}\left(\sum_{i=1}^{n}|s_i|^2\right)^{\frac{1+v_1}{2}} \\ &- \lambda_{\min}\left\{\boldsymbol{K_d}\right\}\left(\sum_{i=1}^{n}|s_i|^2\right)^{\frac{1+v_2}{2}}.\end{aligned} \tag{46}$$

$\boldsymbol{M}_0(\boldsymbol{q})$ can be chosen as

$$\boldsymbol{M}_0(\boldsymbol{q}) = \frac{2}{m_1 + m_2}\boldsymbol{I_n}. \tag{47}$$

Then, the Lyapunov function can be written as

$$V_1 = \frac{1}{m_1 + m_2}\|\boldsymbol{s}\|^2. \tag{48}$$

Applying Eq. (48) to Eq. (46), it follows that

$$\dot{V}_1 \leqslant -\lambda_{\min}\left\{\boldsymbol{K}_p\right\} n^{\frac{1-v_1}{2}} (m_1+m_2)^{\frac{1+v_1}{2}} V_1^{\frac{1+v_1}{2}} - \lambda_{\min}\left\{\boldsymbol{K}_d\right\}(m_1+m_2)^{\frac{1+v_2}{2}} V_1^{\frac{1+v_2}{2}}. \tag{49}$$

According to Lemma 1, due to $v_1 > 1, 0 < v_2 < 1$ are positive constants, the trajectory tracking is fixed-time stable with settling time T_r bounded by Eq. (34).

Step 2. Stability and settling time analysis in sliding phase:

The tracking error of the robotic enters the sliding phase when $\boldsymbol{s} = 0$,

$$\boldsymbol{s} = \dot{\boldsymbol{e}} + \boldsymbol{C}_1\boldsymbol{F}(\boldsymbol{e}) + \boldsymbol{C}_2\mathbf{Sig}^{\beta}(\boldsymbol{e}) = 0. \tag{50}$$

As $\boldsymbol{F}(\boldsymbol{e})$ is a piecewise function of $\boldsymbol{e}$, it can be divided into the following two cases.

Case 1: When $\|\boldsymbol{e}\| \geqslant \delta$, we obtain

$$\dot{\boldsymbol{e}} = -\boldsymbol{C}_1\mathbf{Sig}^{\alpha}(\boldsymbol{e}) - \boldsymbol{C}_2\mathbf{Sig}^{\beta}(\boldsymbol{e}). \tag{51}$$

For Eq. (51), the following Lyapunov function is considered as

$$V_2 = \frac{1}{2}\boldsymbol{e}^T\boldsymbol{e}. \tag{52}$$

Taking the first derivative of Eq. (52), it has

$$V_2 = \boldsymbol{e}^T\dot{\boldsymbol{e}}. \tag{53}$$

After substituting Eq. (50) into (53) yields

$$\begin{aligned}\dot{V}_2 &= \boldsymbol{e}^T\dot{\boldsymbol{e}} = -\boldsymbol{e}^T\boldsymbol{C}_1\mathbf{Sig}^{\alpha}(\boldsymbol{e}) - \boldsymbol{e}^T\boldsymbol{C}_2\mathbf{Sig}^{\beta}(\boldsymbol{e}) \\ &= -\sum_{i=1}^{n} c_{1i}|e_i|^{\alpha+1} - \sum_{i=1}^{n} c_{2i}|e_i|^{\beta+1} \\ &= -\sum_{i=1}^{n} c_{1i}\left(|e_i|^2\right)^{\frac{\alpha+1}{2}} - \sum_{i=1}^{n} c_{2i}\left(|e_i|^2\right)^{\frac{\beta+1}{2}}.\end{aligned} \tag{54}$$

Considering Lemma 2 and $0 < \alpha < 1$, $\beta > 1$, we have

$$\dot{V}_2 \leqslant -\lambda_{\min}(\boldsymbol{C}_1)\|\boldsymbol{e}\|^{\alpha+1} - \lambda_{\min}(\boldsymbol{C}_2) n^{\frac{1-\beta}{2}}\|\boldsymbol{e}\|^{\beta+1}. \tag{55}$$

Substituting Eq. (52) into (55) yields

$$\dot{V}_2 \leqslant -2^{\frac{\alpha+1}{2}}\lambda_{\min}(\boldsymbol{C}_1) V_2^{\frac{\alpha+1}{2}} - 2^{\frac{\beta+1}{2}}\lambda_{\min}(\boldsymbol{C}_2) n^{\frac{1-\beta}{2}} V_2^{\frac{\beta+1}{2}}. \tag{56}$$

By using Lemma 1, the bound of sliding time T_s is given by Eq. (35). It can be obtained that the system tracking errors can reach to an arbitrary small set δ with the bound of T_s.

Case 2: When $\|\boldsymbol{e}\| < \delta$, Eq. (50) can lead to

$$\dot{\boldsymbol{e}} = -\boldsymbol{C}_1\left(k_1\mathbf{Sig}^{r}(\boldsymbol{e}) + k_2\delta^{\|\boldsymbol{e}\|}\boldsymbol{e}\right) - \boldsymbol{C}_2\mathbf{Sig}^{\beta}(\boldsymbol{e}). \tag{57}$$

Then, the Lyapunov function is selected as

$$V_3 = \frac{1}{2}\boldsymbol{e}^T\boldsymbol{e}. \tag{58}$$

Thus,

$$\begin{aligned}\dot{V}_3 &= \boldsymbol{e}^T\dot{\boldsymbol{e}} = -\boldsymbol{C}_1 k_1\mathbf{Sig}^{r}(\boldsymbol{e})\boldsymbol{e} - \boldsymbol{C}_1 k_2\delta^{\|\boldsymbol{e}\|}\boldsymbol{e}^T\boldsymbol{e} - \boldsymbol{C}_2\mathbf{Sig}^{\beta}(\boldsymbol{e})\boldsymbol{e} \\ &\leqslant -k_2\delta^{\|\boldsymbol{e}\|}\lambda_{\min}\{\boldsymbol{C}_1\}\|\boldsymbol{e}\|^2 - k_1\sum_{i=1}^{n} c_{1i}|e_i|^{r+1} - \sum_{i=1}^{n} c_{2i}|e_i|^{\beta+1} \\ &\leqslant -k_2\delta^{\delta}\lambda_{\min}\{\boldsymbol{C}_1\}\|\boldsymbol{e}\|^2 - k_1 n^{(1-r)/2}\lambda_{\min}\{\boldsymbol{C}_1\}\|\boldsymbol{e}\|^{r+1} \\ &\quad - n^{(1-\beta)/2}\lambda_{\min}\{\boldsymbol{C}_2\}\|\boldsymbol{e}\|^{\beta+1} \\ &\leqslant -k_2\delta^{\delta}\lambda_{\min}\{\boldsymbol{C}_1\}\|\boldsymbol{e}\|^2 \\ &= -2k_2\delta^{\delta}\lambda_{\min}\{\boldsymbol{C}_1\} V_3.\end{aligned} \tag{59}$$

According to Lyapunov stability theory, the position tracking error can globally converge to zero exponentially.

Remark 1. According to the stability analysis of Step 1 and Step 2, it can be obtained that the tracking errors of the system can converge firstly to the NFSMC surface $\boldsymbol{s}$ in Eq. (22) within settling time T_r. Then, the tracking errors reach an arbitrary small domain of the origin δ within a fixed-time T_s and thereafter converge to zero exponentially.

Remark 2. The proposed NFSMC scheme can achieve global approximating fixed-time convergence of robotic manipulators with the model uncertainty and bounded external disturbances. However, the proposed control scheme must be formulated with an upper bound on the known coupling uncertainty in advance, and it is always difficult to be satisfied for industrial robotic manipulators.

3.2. Design approach for ANFSMC

In this subsection, an ANFSMC scheme is designed with the unknown upper bound of the coupling uncertainty in Eq. (32). The adaptive switching control law in Eq. (28) can be modified as

$$\begin{aligned}\boldsymbol{\tau}_{a2} &= -\operatorname{sign}(\boldsymbol{s})\,\eta_a \\ \eta_a &= \frac{1}{1-\sigma}\exp\left(\left\|\boldsymbol{M}_0^{-1}(\boldsymbol{q})\right\|^{\varepsilon} - 1\right) \\ &\quad\times\left(\hat{b}_0 + \hat{b}_1\|\boldsymbol{q}\| + \hat{b}_2\|\dot{\boldsymbol{q}}\|^2 + \sigma\|\boldsymbol{\tau}_1 - \boldsymbol{\tau}_0\|\right),\end{aligned} \tag{60}$$

where $\hat{b}_0$, $\hat{b}_1$, and $\hat{b}_2$ are the estimators of b_0, b_1, and b_2, and they are updated by the following laws of adaptability:

$$\dot{\hat{b}}_0 = \mu_0\|\boldsymbol{s}\|, \ \dot{\hat{b}}_1 = \mu_1\|\boldsymbol{s}\|\|\boldsymbol{q}\|, \ \dot{\hat{b}}_2 = \mu_2\|\boldsymbol{s}\|\|\dot{\boldsymbol{q}}\|^2, \tag{61}$$

where μ_0, μ_1, and μ_2 are positive gain constants. Thus,

$$\begin{aligned}\boldsymbol{\tau} &= -\boldsymbol{\tau}_0 + \boldsymbol{\tau}_1 + \boldsymbol{\tau}_{a2} \\ \boldsymbol{\tau}_0 &= \boldsymbol{C}_1\boldsymbol{M}_0\dot{\boldsymbol{F}}(\boldsymbol{e})\dot{\boldsymbol{e}} + \boldsymbol{C}_2\boldsymbol{M}_0\boldsymbol{D}^{\beta-1}(\boldsymbol{e})\dot{\boldsymbol{e}} \\ &\quad - \boldsymbol{C}_0(\boldsymbol{q},\dot{\boldsymbol{q}})\dot{\boldsymbol{q}} - \boldsymbol{G}_0(\boldsymbol{q}) - \boldsymbol{M}_0\ddot{\boldsymbol{q}}_{\boldsymbol{d}} \\ \boldsymbol{\tau}_1 &= -\boldsymbol{K}_{\boldsymbol{p}}\mathbf{Sig}^{v_1}(\boldsymbol{s}) - \boldsymbol{K}_{\boldsymbol{d}}\mathbf{Sig}^{v_2}(\boldsymbol{s}).\end{aligned} \tag{62}$$

Theorem 2. *Considering a robotic manipulator system closed by the controller in Eq. (62), the origin of system tracking error is fixed-time stable.*

Proof. As the ANFSMC and NFSMC schemes have the same sliding mode surface, when the system enters the sliding phase, the ANFSMC scheme has the same convergence properties as NFSMC. The stability of the ANFSMC scheme can be analyzed as follows.

Now, choose a Lyapunov function candidate as

$$V_4 = \frac{1}{2}\boldsymbol{s}^T\boldsymbol{M}_0\boldsymbol{s} + \sum_{i=0}^{2}\frac{1}{2\mu_i}\left(\hat{b}_i - b_i\right)^2. \tag{63}$$

According to Lemma 3 and differentiating V_4 with respect to time yields

$$\dot{V}_4 = \boldsymbol{s}^T\boldsymbol{M}_0\dot{\boldsymbol{s}} + \sum_{i=0}^{2}\frac{1}{\mu_i}\left(\hat{b}_i - b_i\right)\dot{\hat{b}}_i. \tag{64}$$

Substituting Eqs. (37), (61) and (62) into (64), it yields

$$\begin{aligned}\dot{V}_4 =& \boldsymbol{s}^T\left(\boldsymbol{\tau}_1+\boldsymbol{\tau}_{a2}+\boldsymbol{F_d}\right)+\sum_{i=0}^{2}\frac{1}{\mu_i}\left(\hat{b}_i-b_i\right)\dot{\hat{b}}_i\\ =&-\boldsymbol{s}^T\left(\boldsymbol{K_p}\mathbf{Sig}^{v_1}(\boldsymbol{s})+\boldsymbol{K_d}\mathbf{Sig}^{v_2}(\boldsymbol{s})\right)-\|\boldsymbol{s}\|\,\eta_a+\boldsymbol{s}^T\boldsymbol{F_d}\\ &+\left(\left(\hat{b}_0-b_0\right)\|\boldsymbol{s}\|+\left(\hat{b}_1-b_1\right)\|\boldsymbol{s}\|\,\|\boldsymbol{q}\|\right.\\ &+\left.\left(\hat{b}_2-b_2\right)\|\boldsymbol{s}\|\,\|\dot{\boldsymbol{q}}\|^2\right)\\ \leqslant&-(1-\sigma)\|\boldsymbol{s}\|\,\eta_a-\sigma\|\boldsymbol{s}\|\,\eta_a+\|\boldsymbol{s}\|\,\|\boldsymbol{F_d}\|\\ &+\left(\left(\hat{b}_0-b_0\right)+\left(\hat{b}_1-b_1\right)\|\boldsymbol{q}\|+\left(\hat{b}_2-b_2\right)\|\dot{\boldsymbol{q}}\|^2\right)\|\boldsymbol{s}\|\\ &-\boldsymbol{s}^T\left(\boldsymbol{K_p}\mathbf{Sig}^{v_1}(\boldsymbol{s})+\boldsymbol{K_d}\mathbf{Sig}^{v_2}(\boldsymbol{s})\right).\end{aligned} \tag{65}$$

Considering Eqs. (32) and (60), Eqs. (65) can lead to

$$\begin{aligned}\dot{V}_4 \leqslant&-\exp\left(\left\|\boldsymbol{M}_0^{-1}(\boldsymbol{q})\right\|^{\varepsilon}-1\right)\\ &\times\left(\hat{b}_0+\hat{b}_1\|\boldsymbol{q}\|+\hat{b}_2\|\dot{\boldsymbol{q}}\|^2+\sigma\|\boldsymbol{\tau}_1-\boldsymbol{\tau}_0\|\right)\|\boldsymbol{s}\|-\sigma\|\boldsymbol{s}\|\,\eta_a\\ &+\|\boldsymbol{s}\|\left(b_0+b_1\|\boldsymbol{q}\|+b_2\|\dot{\boldsymbol{q}}\|^2+\sigma\|\boldsymbol{\tau}\|\right)\\ &+\left(\left(\hat{b}_0-b_0\right)+\left(\hat{b}_1-b_1\right)\|\boldsymbol{q}\|+\left(\hat{b}_2-b_2\right)\|\dot{\boldsymbol{q}}\|^2\right)\|\boldsymbol{s}\|\\ &-\boldsymbol{s}^T\left(\boldsymbol{K_p}\mathbf{Sig}^{v_1}(\boldsymbol{s})+\boldsymbol{K_d}\mathbf{Sig}^{v_2}(\boldsymbol{s})\right).\end{aligned} \tag{66}$$

According to Eq. (62), we have

$$\|\boldsymbol{\tau}\|\leqslant\|\boldsymbol{\tau}_1-\boldsymbol{\tau}_0\|+\|\boldsymbol{\tau}_{a2}\|. \tag{67}$$

Substituting Eq. (67) into (66), it yields

$$\begin{aligned}\dot{V}_4 \leqslant&-\exp\left(\left\|\boldsymbol{M}_0^{-1}(\boldsymbol{q})\right\|^{\varepsilon}-1\right)\\ &\times\left(\hat{b}_0+\hat{b}_1\|\boldsymbol{q}\|+\hat{b}_2\|\dot{\boldsymbol{q}}\|^2+\sigma\|\boldsymbol{\tau}_1-\boldsymbol{\tau}_0\|\right)\|\boldsymbol{s}\|-\sigma\|\boldsymbol{s}\|\,\eta_a\\ &+\|s\|\left(b_0+b_1\|\boldsymbol{q}\|+b_2\|\dot{\boldsymbol{q}}\|^2+\sigma\|\boldsymbol{\tau}_1-\boldsymbol{\tau}_0\|+\sigma\|\boldsymbol{\tau}_{a2}\|\right)\\ &+\left(\left(\hat{b}_0-b_0\right)+\left(\hat{b}_1-b_1\right)\|\boldsymbol{q}\|+\left(\hat{b}_2-b_2\right)\|\dot{\boldsymbol{q}}\|^2\right)\|\boldsymbol{s}\|\\ &-\boldsymbol{s}^T\left(\boldsymbol{K_p}\mathbf{Sig}^{v_1}(\boldsymbol{s})+\boldsymbol{K_d}\mathbf{Sig}^{v_2}(\boldsymbol{s})\right).\end{aligned} \tag{68}$$

Then, Eq. (68) can be simplified to

$$\begin{aligned}\dot{V}_4 \leqslant&-\exp\left(\left\|\boldsymbol{M}_0^{-1}(\boldsymbol{q})\right\|^{\varepsilon}-1\right)\\ &\times\left(\hat{b}_0+\hat{b}_1\|\boldsymbol{q}\|+\hat{b}_2\|\dot{\boldsymbol{q}}\|^2+\sigma\|\boldsymbol{\tau}_1-\boldsymbol{\tau}_0\|\right)\|\boldsymbol{s}\|\\ &+\sigma\|\boldsymbol{\tau}_1-\boldsymbol{\tau}_0\|\,\|\boldsymbol{s}\|+\left(\hat{b}_0+\hat{b}_1\|\boldsymbol{q}\|+\hat{b}_2\|\dot{\boldsymbol{q}}\|^2\right)\|\boldsymbol{s}\|\\ &-\boldsymbol{s}^T\left(\boldsymbol{K_p}\mathbf{Sig}^{v_1}(\boldsymbol{s})+\boldsymbol{K_d}\mathbf{Sig}^{v_2}(\boldsymbol{s})\right)\\ =&\left(1-\exp\left(\left\|\boldsymbol{M}_0^{-1}(\boldsymbol{q})\right\|^{\varepsilon}-1\right)\right)\left(\hat{b}_0+\hat{b}_1\|\boldsymbol{q}\|+\hat{b}_2\|\dot{\boldsymbol{q}}\|^2\right)\|\boldsymbol{s}\|\\ &+\left(1-\exp\left(\left\|\boldsymbol{M}_0^{-1}(\boldsymbol{q})\right\|^{\varepsilon}-1\right)\right)\sigma\|\boldsymbol{\tau}_1-\boldsymbol{\tau}_0\|\,\|\boldsymbol{s}\|\\ &-\boldsymbol{s}^T\left(\boldsymbol{K_p}\mathbf{Sig}^{v_1}(\boldsymbol{s})+\boldsymbol{K_d}\mathbf{Sig}^{v_2}(\boldsymbol{s})\right).\end{aligned} \tag{69}$$

Considering $\exp\left(\left\|\boldsymbol{M}_0^{-1}(\boldsymbol{q})\right\|^{\varepsilon}-1\right)\geqslant 1$, one can obtain

$$\dot{V}_4\leqslant-\boldsymbol{s}^T\left(\boldsymbol{K_p}\mathbf{Sig}^{v_1}(\boldsymbol{s})+\boldsymbol{K_d}\mathbf{Sig}^{v_2}(\boldsymbol{s})\right). \tag{70}$$

Compared with Eq. (43), it can be obtained that the ANFSMC scheme has the same setting time as the NFSMC scheme, which means that the desired tracking can be achieved, and hence the proof is completed.

Remark 3. In the proof of setting time, the mathematical development including inequalities results that the bound of setting time is conservation. Worth to be mentioned, the non-singularity of the system is realized at the expense of the convergence accuracy.

3.3. Design approach for ANFSMC under actuator saturation

Fixed-time SMC always requires a fast transient response with large torque, which may result in actuator saturation. As an auxiliary system, saturation compensator is an effective method to compensate or weaken the negative effects of saturation. Therefore, a saturation compensator is designed for the ANFSMC scheme in this subsection.

Let $\boldsymbol{u}_c$ be the input of the control system, $\boldsymbol{u}_{\max}$ be the saturation value. Saturation function defined in Eq. (3) is always used to formulate the control input constraints, then $\Delta\boldsymbol{u}_c=\boldsymbol{u}_c-\mathrm{sat}(\boldsymbol{u}_c)$ denotes the saturation error. The auxiliary variable $\boldsymbol{\zeta}\in R^{n\times 1}$ and the auxiliary matrix $\boldsymbol{\Gamma}\in R^{n\times n}$ can be obtained from the following auxiliary system

$$\dot{\zeta}=\begin{cases}0,\ \|\zeta\|<\zeta_0\\ -k_a\mathbf{Sig}^{\beta}(\zeta)-k_b\mathbf{Sig}^{\alpha}(\zeta)-\dfrac{\left\|\boldsymbol{s}^T\boldsymbol{\Omega}^{-1}\Gamma\right\|+\frac{1}{2}\left(\Delta\boldsymbol{u}_c^T\Delta\boldsymbol{u}_c+k_a\zeta^T\zeta\right)}{\|\zeta\|^2}\zeta\\ \quad+k_c\Delta\boldsymbol{u}_c,\ \|\zeta\|>\zeta_0\end{cases} \tag{71}$$

$$\Gamma=\mathrm{diag}\left\{\dot{e}_i^{1-\alpha}\Delta u_{ci}\right\},\ i=1,2,\ldots,n, \tag{72}$$

where α and β are positive constants defined in Eqs. (17) and (23), $\boldsymbol{s}$ is the proposed sliding mode surface in Eq. (22), k_a, k_b, k_c are positive constants with $0<k_c<k_a<1$. $\boldsymbol{\Omega}\in R^{n\times n}$ is a known symmetric positive matrix.

Remark 4. The auxiliary variable can achieve saturation compensator fixed-time convergence of the tracking control. By selecting the appropriate parameter k_c, the possible overcompensation of actuator saturation can be avoided.

The fixed-time compensation for input saturation is designed as

$$\boldsymbol{\tau}_{sa}=-\boldsymbol{K_d}\boldsymbol{M}_0^{-1}(\boldsymbol{q})\,\boldsymbol{\zeta}, \tag{73}$$

where $\boldsymbol{K_d}$ is the positive-definite diagonal matrix defined in Eq. (27). The controller of ANFSMC-AS can be written as

$$\begin{aligned}\boldsymbol{\tau}&=\boldsymbol{\tau}_0+\boldsymbol{\tau}_1+\boldsymbol{\tau}_2+\boldsymbol{\tau}_{sa}\\ \boldsymbol{\tau}_0&=\boldsymbol{C}_1\boldsymbol{M}_0\dot{\boldsymbol{F}}(\boldsymbol{e})\dot{\boldsymbol{e}}+\boldsymbol{C}_2\boldsymbol{M}_0\boldsymbol{D}^{\beta-1}(\boldsymbol{e})\dot{\boldsymbol{e}}\\ &\quad-\boldsymbol{C}_0(\boldsymbol{q},\dot{\boldsymbol{q}})\dot{\boldsymbol{q}}-\boldsymbol{G}_0(\boldsymbol{q})-\boldsymbol{M}_0\ddot{\boldsymbol{q}}_{\boldsymbol{d}}\\ \boldsymbol{\tau}_1&=-\boldsymbol{K_p}\mathbf{Sig}^{v_1}(\boldsymbol{s})-\boldsymbol{K_d}\mathbf{Sig}^{v_2}(\boldsymbol{s})\\ \boldsymbol{\tau}_2&=-\frac{\mathrm{sign}(\boldsymbol{s})}{1-\sigma}\exp\left(\left\|\boldsymbol{M}_0^{-1}(\boldsymbol{q})\right\|^{\varepsilon}-1\right)\\ &\quad\times\left(\hat{b}_0+\hat{b}_1\|\boldsymbol{q}\|+\hat{b}_2\|\dot{\boldsymbol{q}}\|^2+\sigma\|\boldsymbol{\tau}_1-\boldsymbol{\tau}_0\|\right).\end{aligned} \tag{74}$$

Theorem 3. *With the saturation compensator in Eq. (73), the controller in Eq. (74) can realize the effective compensation for the saturation of the actuator and ensure that the system is fixed-time stable.*

Proof. Propose the following Lyapunov function as

$$V_5=\frac{1}{2}\zeta^T\zeta. \tag{75}$$

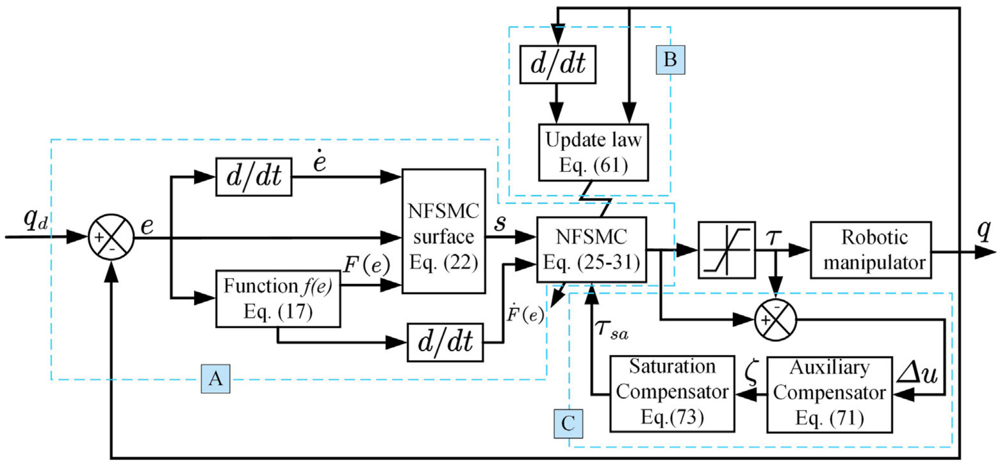

Fig. 1. Control flowchart of the proposed ANFSMC-AS.

Differentiating V_5 with respect to time and using Eq. (71) yields

$$\begin{aligned}\dot{V}_5 =& \boldsymbol{\zeta}^T\dot{\boldsymbol{\zeta}} = -k_a\boldsymbol{\zeta}^T\mathbf{Sig}^{\beta}(\boldsymbol{\zeta}) - k_b\boldsymbol{\zeta}^T\mathbf{Sig}^{\alpha}(\boldsymbol{\zeta}) - \left\|\boldsymbol{s}^T\boldsymbol{\Omega}^{-1}\boldsymbol{\Gamma}\right\| \\ & -\frac{1}{2}\Delta\boldsymbol{u}_c^T\Delta\boldsymbol{u}_c - \frac{1}{2}k_a\boldsymbol{\zeta}^T\boldsymbol{\zeta} + k_c\boldsymbol{\zeta}^T\Delta\boldsymbol{u}_c \\ \leqslant& -k_a\boldsymbol{\zeta}^T\mathbf{Sig}^{\beta}(\boldsymbol{\zeta}) - k_b\boldsymbol{\zeta}^T\mathbf{Sig}^{\alpha}(\boldsymbol{\zeta}) - \frac{1}{2}\Delta\boldsymbol{u}_c^T\Delta\boldsymbol{u}_c \\ & -\frac{1}{2}k_a\boldsymbol{\zeta}^T\boldsymbol{\zeta} + k_c\boldsymbol{\zeta}^T\Delta\boldsymbol{u}_c.\end{aligned} \tag{76}$$

According to the following inequalities

$$\boldsymbol{\zeta}^T\Delta\boldsymbol{u}_c \leqslant \frac{1}{2}\boldsymbol{\zeta}^T\boldsymbol{\zeta} + \frac{1}{2}\Delta\boldsymbol{u}_c^T\Delta\boldsymbol{u}_c \tag{77}$$

Then, $\dot{V}_5$ can be written as

$$\begin{aligned}\dot{V}_5 \leqslant& -k_a\boldsymbol{\zeta}^T\mathbf{Sig}^{\beta}(\boldsymbol{\zeta}) - k_b\boldsymbol{\zeta}^T\mathbf{Sig}^{\alpha}(\boldsymbol{\zeta}) \\ & -\frac{1}{2}\Delta\boldsymbol{u}_c^T\Delta\boldsymbol{u}_c - \frac{1}{2}k_a\boldsymbol{\zeta}^T\boldsymbol{\zeta} + \frac{1}{2}k_c\boldsymbol{\zeta}^T\boldsymbol{\zeta} + \frac{1}{2}k_c\Delta\boldsymbol{u}_c^T\Delta\boldsymbol{u}_c \\ =& -k_a\boldsymbol{\zeta}^T\mathbf{Sig}^{\beta}(\boldsymbol{\zeta}) - k_b\boldsymbol{\zeta}^T\mathbf{Sig}^{\alpha}(\boldsymbol{\zeta}) \\ & -\frac{1}{2}(k_a - k_c)\boldsymbol{\zeta}^T\boldsymbol{\zeta} - \frac{1}{2}(1 - k_c)\Delta\boldsymbol{u}_c^T\Delta\boldsymbol{u}_c.\end{aligned} \tag{78}$$

Considering that $0 < k_c < k_a < 1$, we can obtain that

$$\begin{aligned}\dot{V}_5 \leqslant& -k_a\boldsymbol{\zeta}^T\mathbf{Sig}^{\beta}(\boldsymbol{\zeta}) - k_b\boldsymbol{\zeta}^T\mathbf{Sig}^{\alpha}(\boldsymbol{\zeta}) \\ =& -k_a\sum_{i=1}^{n}(\zeta_i)^{\beta+1} - k_b\sum_{i=1}^{n}(\zeta_i)^{\alpha+1},\end{aligned} \tag{79}$$

where ζ_i denotes the ith elements of the auxiliary variable $\boldsymbol{\zeta}$. Considering Lemma 2, Eq. (79) can lead to

$$\dot{V}_5 \leqslant -2^{\beta-1}k_aV_5^{\beta} - 2^{(\alpha+1)/2}k_bV_5^{(\alpha+1)/2}. \tag{80}$$

Substituting Eq. (75) into Eq. (80), it yields

$$\dot{V}_5 \leqslant -n^{(1-\beta)/2}2^{(\beta+1)/2}k_aV_5^{(\beta+1)/2} - 2^{(\alpha+1)/2}k_bV_5^{(\alpha+1)/2}. \tag{81}$$

Since $\beta > 1$ and $\alpha < 1$, by Lemma 1, it can obtain that the saturation compensator is fixed-time stable, and the convergence time can be written as

$$T_{as} \leqslant \frac{n^{(\beta-1)/2}2^{(1-\beta)/2}}{k_a(\beta-1)} + \frac{2^{(1-\alpha)/2}}{k_b(1-\alpha)}. \tag{82}$$

This completes the proof.

Remark 5. The actuator saturation compensator only works when the actuator is saturated. Compared with the method of using bounded control to avoid saturation to make the system asymptotically stable, it does not affect the performance of the ANFSMCer. But it is worth noting that the actuator saturation compensator can only be used to weaken the impact of saturation on the system, and cannot completely offset the effect of actuator saturation.

Remark 6. In this paper, the control input of the actuator is not allowed to exceed the allowable value in a wide range or the saturation time is too long so that the actual output control torque can provide sufficient driving torque to guarantee the robotic manipulator can execute a given tracking task. Otherwise, the robotic manipulator will become an underactuated one, and the controller needs to be redesigned. In addition, the transient response of the robotic manipulator is positively correlated to the range of the control torque. When the actuator of the robotic manipulator is saturated, the gain parameters of the controller should be adjusted to increase the convergence time of the tracking error and try to avoid the saturation of the actuator.

Remark 7. When implementing the proposed control scheme, control parameters should be carefully selected to achieve fast transients and high tracking accuracy of robotic manipulators. The control parameters mainly include two types. One is the parameters determined by the characteristics of the robotic manipulator, including m_1 and m_2. The other type of parameters is used to determine the performance of the controller, including the positive constants $\upsilon_1, \upsilon_2, \delta, \varepsilon, \beta$, control gain matrixes $\boldsymbol{C}_1, \boldsymbol{C}_2, \boldsymbol{K_p}, \boldsymbol{K_d}$, gain constants of actuator saturation compensator k_a, k_b, k_c and auxiliary actuator matrix $\boldsymbol{\Omega}$. In general, positive constants $\upsilon_1, \upsilon_2, \varepsilon$ and β can be chosen as $\upsilon_1 = 2.5$, $\upsilon_2 = 0.5$, $\varepsilon = 0.01$ and $\beta = 1.9$ for most robotic manipulator systems. A small δ contributes to fast transient but too small δ may conduce large overshoot and more energy consumption. Control gain matrixes $\boldsymbol{C}_1, \boldsymbol{C}_2, \boldsymbol{K_p}$ and $\boldsymbol{K_d}$ should be chosen as large as possible for fast transient and higher tracking accuracy. However, excessively large control gain matrixes can also cause actuator saturation. For actuator saturation compensator, auxiliary actuator matrix $\boldsymbol{\Omega}$ always can be chosen as $\boldsymbol{\Omega} = 0.5\boldsymbol{I}_2$. Larger gain constants k_a and k_b can improve the effect of saturation compensation. However, large gain constants may cause the actuator to overcompensate, and the possible overcompensation of actuator saturation can be avoided by increasing k_c.

A flowchart of the ANFSMC-AS scheme is presented in Fig. 1. **Part A** is the NFSMC controller designed in Section 3.1, **Part B** is the adaptive controller designed in Section 3.2, and **Part C** is the actuator saturation compensator designed in Section 3.3.

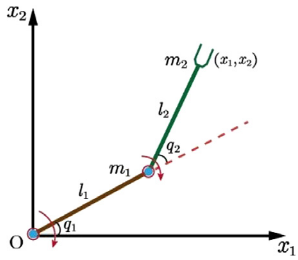

Fig. 2. Architecture of a two-link robotic manipulator.

4. Simulation results

To demonstrate the effectiveness of the proposed control schemes, a two-link manipulator shown in Fig. 2 is considered. The dynamics of two-link robotic manipulators are given by [29]

$$\begin{bmatrix} M_{11}(q) & M_{12}(q) \\ M_{21}(q) & M_{22}(q) \end{bmatrix} \begin{bmatrix} \ddot{q}_1 \\ \ddot{q}_2 \end{bmatrix} + \begin{bmatrix} C_{11}(q) & C_{12}(q) \\ C_{21}(q) & C_{22}(q) \end{bmatrix} \begin{bmatrix} \dot{q}_1 \\ \dot{q}_2 \end{bmatrix} + \begin{bmatrix} G_1(q) \\ G_2(q) \end{bmatrix} = \begin{bmatrix} \tau_1 \\ \tau_2 \end{bmatrix} \tag{83}$$

$$\text{where} \quad \begin{aligned} & M_{11}(q) = (m_1 + m_2) l_1^2 + m_2 l_2^2 + 2 m_2 l_1 l_2 \cos(q_2) + I_1 \\ & M_{12}(q) = M_{21}(q) = m_2 l_2^2 + m_2 l_1 l_2 \cos(q_2) \\ & M_{22}(q) = m_2 l_2^2 + I_2 \\ & C_{11}(q, \dot{q}) = -2 m_2 l_1 l_2 \sin(q_2) \dot{q}_2 \\ & C_{12}(q, \dot{q}) = -m_2 l_1 l_2 \sin(q_2) \dot{q}_2 \\ & C_{21}(q, \dot{q}) = m_2 l_1 l_2 \sin(q_2) \dot{q}_1 \\ & C_{22}(q, \dot{q}) = 0 \\ & G_1(q) = (m_1 + m_2) g l_1 \cos(q_1) + m_2 g l_2 \cos(q_1 + q_2) \\ & G_2(q) = m_2 l_2 g \cos(q_1 + q_2). \end{aligned}$$

The model parameters of the manipulator are set as: $l_1 = 1$ m, $l_2 = 0.8$ m, $m_1 = 0.5$ kg, $m_2 = 1.5$ kg, $I_1 = 5$ kg $\cdot$ m^2, $I_2 = 5$ kg $\cdot$ m^2, where l_i is the length of link i, m_i is the mass of link i, and I_i is the inertia of link i, $i = 1, 2$. Gravitational acceleration is $g = 9.81$ m/s^2. The nominal values of m_1, m_2 are $m_1^0 = 0.6$ kg, $m_2^0 = 1.8$ kg and the nominal values of I_1, I_2 are $I_1^0 = 6$ kg $\cdot$ m^2, $I_2^0 = 6$ kg $\cdot$ m^2. All numerical simulations in this paper are conducted with the following external disturbances

$$\boldsymbol{\tau}_d(t) = \begin{bmatrix} \tau_{1d}(t) \\ \tau_{2d}(t) \end{bmatrix} = \begin{bmatrix} 2\sin(t) + 0.5\sin(200\pi t) \\ \cos(2t) + 0.5\sin(200\pi t) \end{bmatrix}. \tag{84}$$

The reference trajectories $\boldsymbol{q}_d = [q_{d1}, q_{d2}]^T$ are designed as [29]

$$\begin{aligned} q_{d1} &= 1.25 - \frac{7}{5}\exp(-t) + \frac{7}{20}\exp(-4t) \\ q_{d2} &= 1.25 + \exp(-t) - \frac{1}{4}\exp(-4t). \end{aligned} \tag{85}$$

The initial conditions of the system are set to $q_1(0) = 1$, $q_2(0) = 1.5$, $\dot{q}_1(0) = 0$, $\dot{q}_2(0) = 0$. The parameters of the proposed controllers are listed in Table 1.

Four sets of simulations are described in this paper. First, we discuss the NFSMC scheme described in Section 3.1, where the upper bound of the coupling uncertainties $\boldsymbol{F}_d$ is assumed to be known. Second, the ANFSMC scheme in Section 3.2 with unknown uncertainties $\boldsymbol{F}_d$ is simulated. Comparative studies between ANFSMC and three other SMC schemes are then presented. Finally, considering the case of actuator saturation, ANFSMC-AS is simulated and compared with the controller without saturation compensation.

4.1. Performance evaluation of NFSMC

Simulation results for the NFSMC scheme proposed in Section 3.1 are displayed in Figs. 3–7. Figs. 3 and 4 show the position

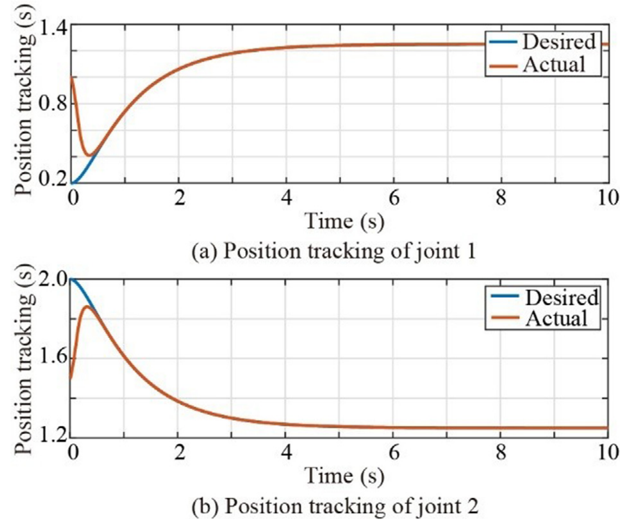

Fig. 3. Position tracking performance.

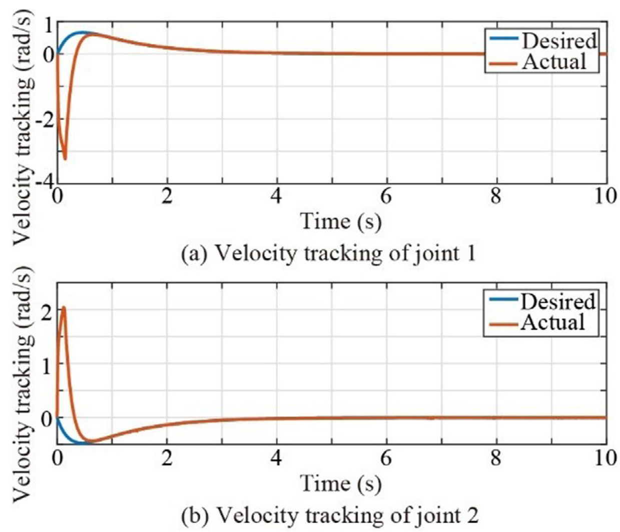

Fig. 4. Velocity tracking performance.

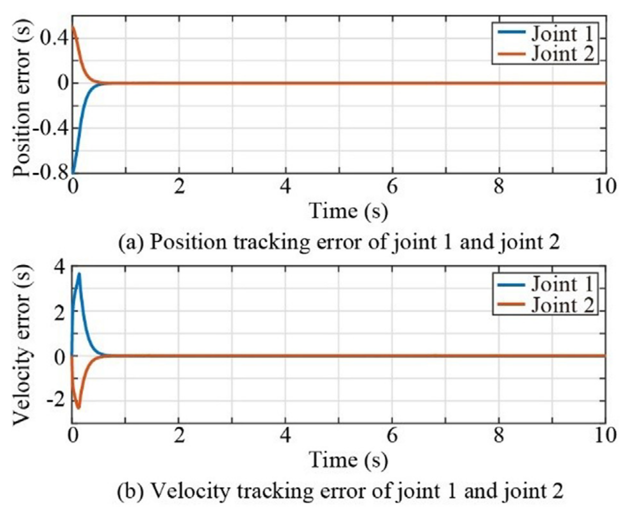

Fig. 5. Position and velocity tracking errors.

Table 1
Parameters of the controllers.

Parameter	Value	Parameter	Value
Positive constant m_1	0.2	Positive constant m_2	0.09
Positive constant υ_1	2.5	Positive constant υ_2	0.5
Positive constant ε	0.001	Positive constant δ	0.3
Tracking gain error β	1.9	Auxiliary system constant b_0	9.5
Auxiliary system constant b_1	2.2	Auxiliary system constant b_1	2.8
Adaptive constant λ	0.67	Auxiliary actuator constant k_a	0.5
Auxiliary actuator constant k_b	1	Auxiliary actuator constant k_c	0.2
Auxiliary actuator matrix $\boldsymbol{\Omega}$	$0.5\boldsymbol{I}_2$	Control gain matrixes $\boldsymbol{C}_1, \boldsymbol{C}_2, \boldsymbol{K_p}, \boldsymbol{K_d}$	$5\boldsymbol{I}_2$

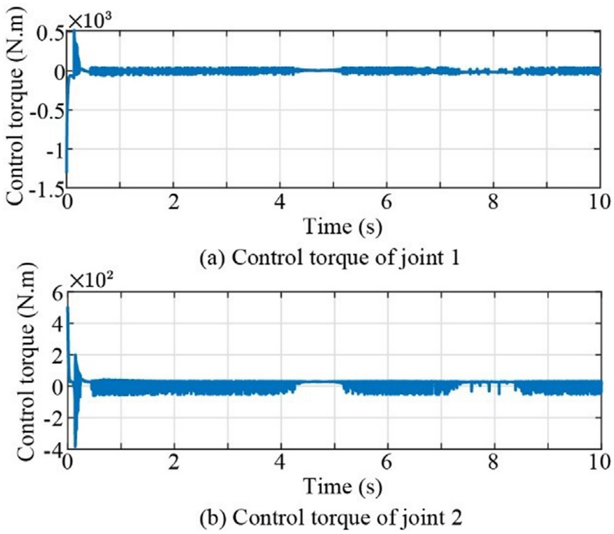

Fig. 6. Control torque of joints 1 and 2.

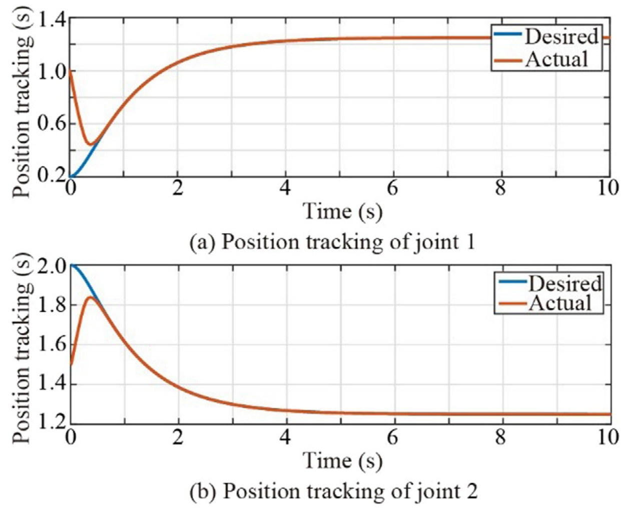

Fig. 8. Position tracking performance.

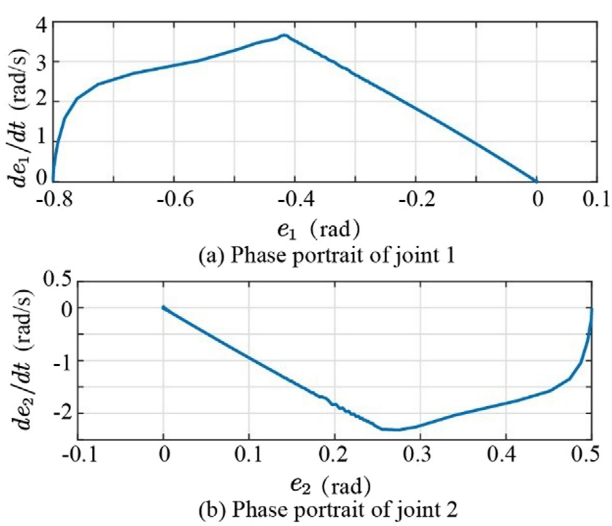

Fig. 7. Phase portraits of joints 1 and 2.

and speed tracking performance of the proposed NFSMC scheme, and Fig. 5 shows the position and speed tracking errors of the robotic manipulator. These results demonstrate that the robotic manipulator can quickly and accurately track the desired trajectories and desired velocity under an uncertain external disturbance. Fig. 6 presents the control torque of joints 1 and 2. To achieve fast track of the ideal trajectories, the control torque of the robotic manipulator has a large transient response at the beginning of the movement. Fig. 7 shows the phase diagram of joints 1 and 2. The proposed control system can reach the sliding surface with a limited time, and then converges to zero along this surface. Therefore, the proposed NFSMC scheme achieves fast transients in the manipulator with highly stable tracking accuracy, avoids singularities, and it has strong robustness to interference and system uncertainties.

4.2. Performance evaluation of ANFSMC

Simulation results using the ANFSMC scheme proposed in Section 3.2 are shown in Figs. 8–13. For initial conditions of $\hat{b}_0 = 0, \hat{b}_1 = 0, \hat{b}_2 = 0$, Figs. 8 and 9 present the position and velocity tracking performance of the proposed ANFSMC scheme. Fig. 10 shows the position and velocity tracking errors of the manipulator, demonstrating that the manipulator can achieve excellent trajectory tracking performance. From Fig. 11, it can be seen that the input joint control torque is smooth, which is beneficial to the manipulator in practical applications. Moreover, the adaptive system is insensitive to disturbances and the model uncertainties. Fig. 12 shows the phase diagrams of joints 1 and 2, illustrating that the proposed control scheme achieves good convergence. Fig. 13 shows that the predicted values of the parameters in the adaptive system rapidly converge to constants. These simulation results show that the proposed ANFSMC can maintain good control performance when the upper bound of the lumped uncertainty is unknown, and even obtain a smoother control torque input than the NFSMC scheme.

4.3. ANFSMC comparative study

To prove the superiority of the proposed ANFSMC scheme, the results given by SFSMC [19], ANFTSMC [29], and FNTSMC [8] are compared with from the proposed scheme. All simulations use

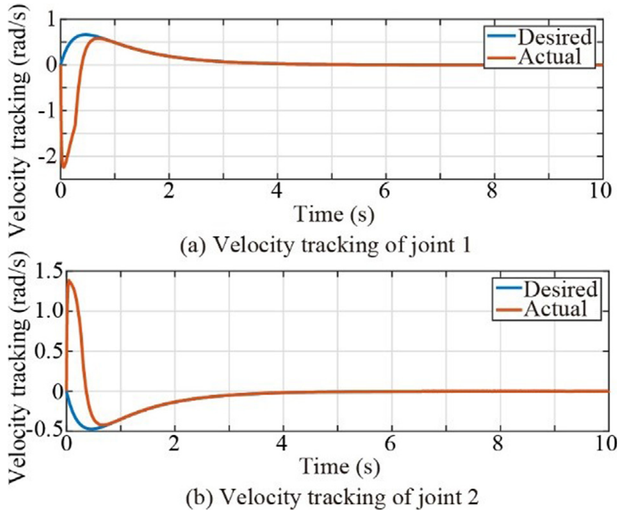

Fig. 9. Velocity tracking performance.

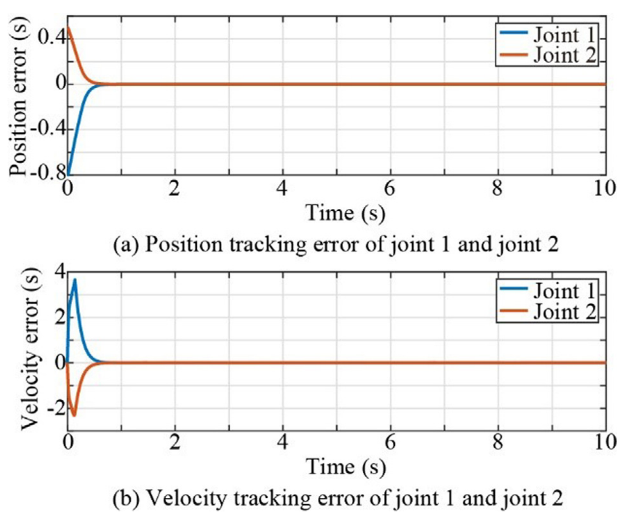

Fig. 10. Position and velocity tracking errors.

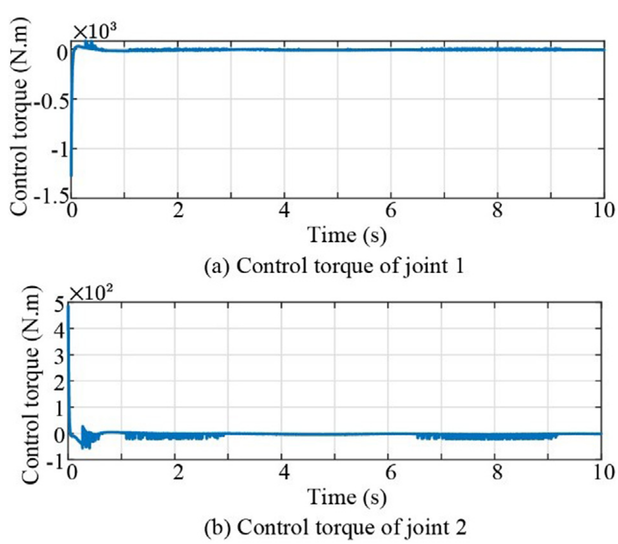

Fig. 11. Control torque of joints 1 and 2.

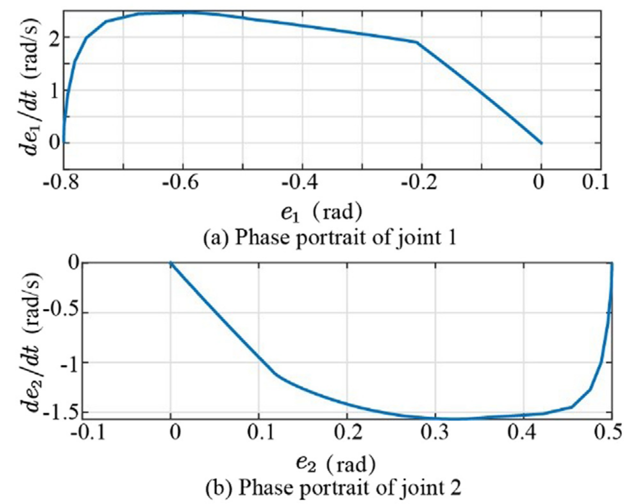

Fig. 12. Phase portraits of joints 1 and 2.

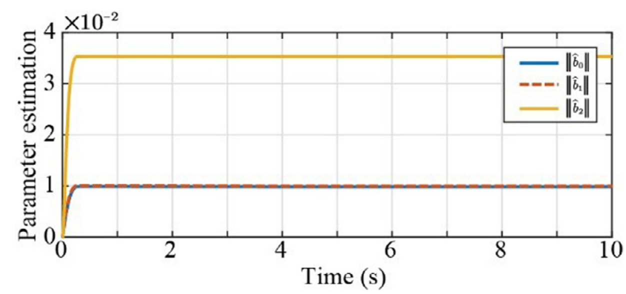

Fig. 13. Parameter estimation.

the same tracking trajectory and the robotic manipulator parameters in [8,19,29] to ensure that the comparison is reasonable. The SFSMCer can be described as follows [19]:

$$
\begin{aligned}
&\boldsymbol{\tau} = -\boldsymbol{\eta} + \boldsymbol{\tau}_0 + \boldsymbol{\tau}_1 \\
&\boldsymbol{\eta} = \boldsymbol{C}_1\boldsymbol{M}_0\boldsymbol{B}(\boldsymbol{e})\dot{\boldsymbol{e}} + \boldsymbol{C}_2\boldsymbol{M}_0\boldsymbol{D}^{\beta-1}(\boldsymbol{e})\dot{\boldsymbol{e}} \\
&\qquad - \boldsymbol{C}_0(\boldsymbol{q},\dot{\boldsymbol{q}})\dot{\boldsymbol{q}} - \boldsymbol{g}_0(\boldsymbol{q}) - \boldsymbol{M}_0\ddot{\boldsymbol{q}}_{\boldsymbol{d}} \\
&\boldsymbol{\tau}_0 = -\boldsymbol{K}_1\mathbf{Sig}^{\upsilon_1}(\boldsymbol{s}) - \boldsymbol{K}_2\mathbf{Sig}^{\upsilon_2}(\boldsymbol{s}) \\
&\boldsymbol{\tau}_1 = -b(\boldsymbol{s})\cdot\frac{1}{1-\sigma}\left(a_0 + a_1\|\dot{\boldsymbol{q}}\|^2 + \sigma\|\boldsymbol{\tau}_0 - \boldsymbol{\eta}\|\right) \\
&\boldsymbol{s} = \dot{\boldsymbol{e}} + \boldsymbol{C}_1\boldsymbol{F}(\boldsymbol{e}) + \boldsymbol{C}_2\mathbf{Sig}^{\beta}(\boldsymbol{e}) \\
&f(e) = \begin{cases} k_a\mathrm{sig}^{\alpha+1}(x) + k_b\delta^{|x|}x, \text{ if } |x| < \delta \\ \mathrm{sig}^{1-\delta}(x), \text{ if } |x| \geqslant \delta \end{cases} \\
&\boldsymbol{F}(\boldsymbol{e}) = [f(e_i)]^T, i = 1, 2, \ldots, n \\
&\boldsymbol{B}(\boldsymbol{e}) = \mathrm{diag}\left\{\dot{f}(e_i)\right\}, i = 1, 2, \ldots, n \\
&b(\boldsymbol{s}) = \begin{cases} \frac{\boldsymbol{s}}{\|\boldsymbol{s}\|}, \|\boldsymbol{s}\| \neq 0 \\ 0, \|\boldsymbol{s}\| = 0 \end{cases}
\end{aligned}
\tag{86}
$$

where $\delta, \beta, \upsilon_1, \upsilon_2, a_0, a_1$ are positive coefficients and $\boldsymbol{C}_1, \boldsymbol{C}_2, \boldsymbol{K}_1, \boldsymbol{K}_2$ are positive-definite diagonal matrices.

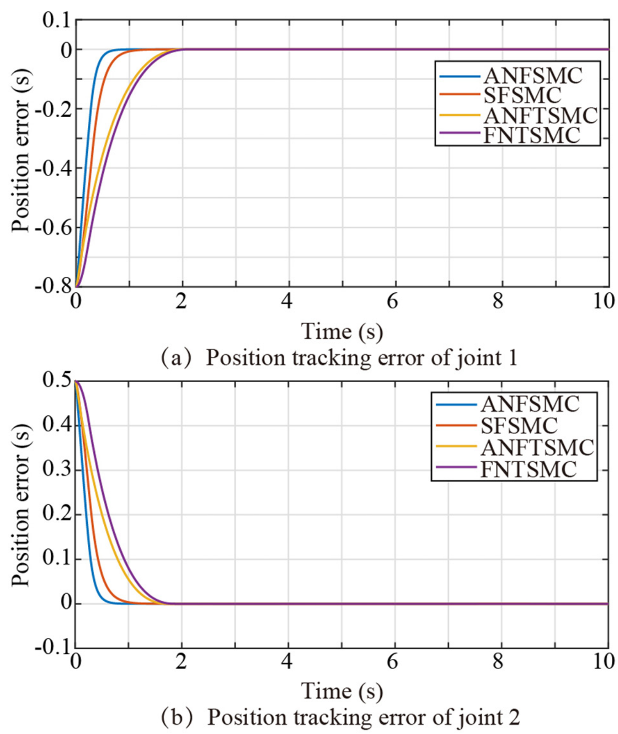

Fig. 14. Position tracking error performance.

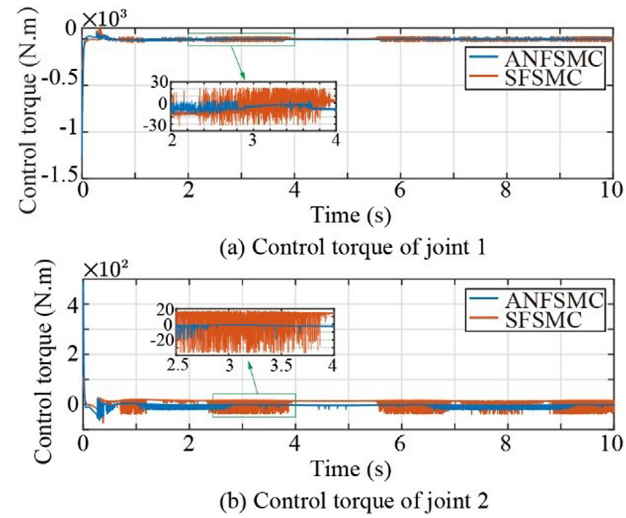

Fig. 15. ANFSMC and SFSMC control torque.

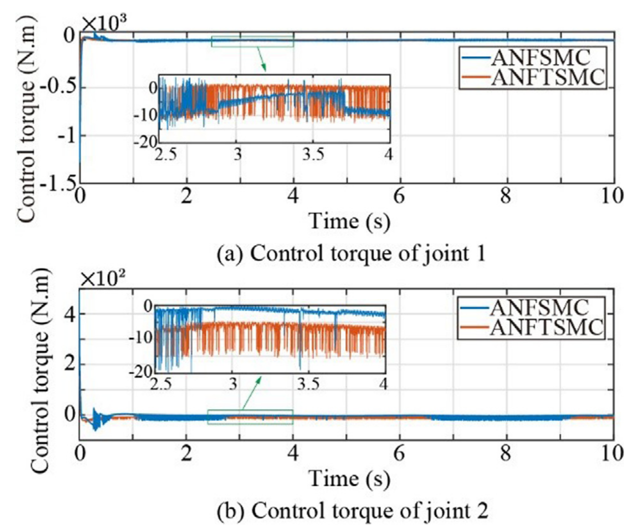

Fig. 16. ANFSMC and ANFTSMC control torque.

The control laws of ANFTSMC are given by [29]

$$\begin{aligned}
s(t) &= \varepsilon_1 + k_1 |e|^{\alpha} \operatorname{sign}(e) + k_2 |\dot{e}|^{\beta} \operatorname{sign}(\dot{e}) \\
\boldsymbol{\tau}(t) &= \boldsymbol{\tau}_{eq}(t) + \boldsymbol{\tau}_{asw}(t) \\
\boldsymbol{\tau}_{eq}(t) &= \boldsymbol{M}_0(\boldsymbol{q})\ddot{\boldsymbol{q}}_{\boldsymbol{d}} + \boldsymbol{C}_0(\boldsymbol{q},\dot{\boldsymbol{q}})\dot{\boldsymbol{q}} + \boldsymbol{G}_0(\boldsymbol{q}) \\
&\quad - \frac{\boldsymbol{M}_0(\boldsymbol{q})}{\beta \cdot k_2} |\dot{e}|^{2-\beta}\left(1 + \alpha \cdot k_1 |e|^{\alpha-1}\right)\operatorname{sign}(\dot{e}) \\
\boldsymbol{\tau}_{asw}(t) &= -\boldsymbol{M}_0(q)\left[k \cdot s + \left(\widehat{b}_0 + \widehat{b}_1|q| + \widehat{b}_2|\dot{q}|^2 + \eta\right)\operatorname{sign}(s)\right] \\
\hat{b}_0 &= \lambda_0|s| \cdot |\dot{e}|^{\beta-1} \\
\hat{b}_1 &= \lambda_1|s| \cdot |\dot{e}|^{\beta-1}|q| \\
\hat{b}_2 &= \lambda_2|s| \cdot |\dot{e}|^{\beta-1}|\dot{q}|^2
\end{aligned} \tag{87}$$

where $\alpha, \beta, \eta, k_1, k_2, k, \lambda_0, \lambda_1, \lambda_2$ are positive coefficients.

The FNTSMC scheme is written as [8]

$$\begin{aligned}
\boldsymbol{S} &= \boldsymbol{e} + \mathbf{Sig}^{\boldsymbol{\Gamma}_1}(\boldsymbol{e}) + \mathbf{Sig}^{\boldsymbol{\Gamma}_2}(\dot{\boldsymbol{e}}) \\
\boldsymbol{\tau} &= -\boldsymbol{M}_{\boldsymbol{0}}(\boldsymbol{q})\left[M_2\boldsymbol{S} + (\boldsymbol{S} + M_1)\frac{\boldsymbol{S}}{\|\boldsymbol{S}\|} + \boldsymbol{F}_2\right. \\
&\quad \left. + \boldsymbol{\Gamma}_2^{-1}\left(\boldsymbol{I}_2 + \boldsymbol{\Gamma}_1\boldsymbol{D}^{\boldsymbol{\Gamma}_1-\boldsymbol{I}_2}(\boldsymbol{e})\right)\mathbf{Sig}^{2\boldsymbol{I}_2-\boldsymbol{\Gamma}_2}(\dot{\boldsymbol{e}})\right] \\
\zeta &= \left\|\boldsymbol{M}_{\boldsymbol{0}}^{-1}(\boldsymbol{q})\right\|\left(b_0 + b_1|\boldsymbol{q}| + b_2|\dot{\boldsymbol{q}}|^2\right) \\
\boldsymbol{F}_2 &= -\boldsymbol{M}_0^{-1}(\boldsymbol{q})\left(\boldsymbol{C}(\boldsymbol{q},\dot{\boldsymbol{q}}) + \boldsymbol{g}_{\boldsymbol{0}}(\boldsymbol{q})\right) - \ddot{\boldsymbol{q}}_{\boldsymbol{d}},
\end{aligned} \tag{88}$$

where b_0, b_1, b_2, M_1, M_2 are known positive constants, $\boldsymbol{\Gamma}_1$ and $\boldsymbol{\Gamma}_2$ are two given positive-definite diagonal matrices.

The control parameters for these three schemes are listed in Table 2, and are the same as in their respective papers [8,19,29].

Fig. 14 presents the position tracking error with the different controllers. The trajectory tracking error of the developed control scheme converges to zero faster than in the other control schemes. Figs. 15–17 provide a clear comparison of the joint torques with the various controllers. In the case of external disturbances, the proposed scheme provides a smaller control torque chattering and smoother control input. To ulteriorly compare the trajectory tracking and control torque output performance of the four controllers, the integrated absolute error (IAE), the energy of control input (ECI), and absolute input chattering error (AICE) are designed as

$$|e_i|_{\mathrm{IAE}} = \frac{1}{N}\sum_{k=1}^{N}|e_i(k)| \tag{89}$$

$$|\tau_i|_{\mathrm{ECI}} = \frac{1}{N}\sum_{k=1}^{N}|\tau_i(k)| \tag{90}$$

$$|\varDelta\tau_i|_{\mathrm{AICE}} = \frac{1}{N}\sum_{k=1}^{N-1}|\tau_i(k+1) - \tau_i(k)|, \tag{91}$$

where N is the total number of samples, i denotes the joint number, and $e(k)$, $\tau(k)$ denote the position error and control input of joints, respectively.

As shown in Figs. 18–20, the proposed ANFSMC scheme gives smaller values of IAE and ECI than the other controllers. In Fig. 20, the ANSTSMC controller achieves a slightly smaller AICE value

Table 2
Parameter values of SFSMC, ANFTSMC, and FNTSMC.

Controller	Parameters
SFSMC [18]	$\delta = 0.3,\ \alpha = 0.7,\ r = 1.7,\ \beta = 1.9,\ \boldsymbol{C}_1 = \boldsymbol{C}_2 = 3\boldsymbol{I}_2$ $\boldsymbol{K}_1 = \boldsymbol{K}_2 = 5\boldsymbol{I}_2,\ \nu_1 = 2.5,\ \nu_2 = 0.5,\ a_0 = 12,\ a_1 = 2.2$
ANFTSMC [29]	$\alpha = 0.2,\ \beta = 5/3,\ \eta = 0.5,\ k = 250,\ \lambda_0 = \lambda_1 = \lambda_2 = 0.01$ $k_1 = k_2 = 1,\ \hat{b}_0(0) = \hat{b}_1(0) = \hat{b}_2(0) = 0$
FNTSMC [8]	$\boldsymbol{\Gamma}_1 = \mathrm{diag}\{2, 2\},\ M_1 = M_2 = 2,\ \boldsymbol{\Gamma}_2 = \mathrm{diag}\{5/3, 5/3\}$ $b_0 = 12,\ b_1 = 2.2,\ b_2 = 2.8$

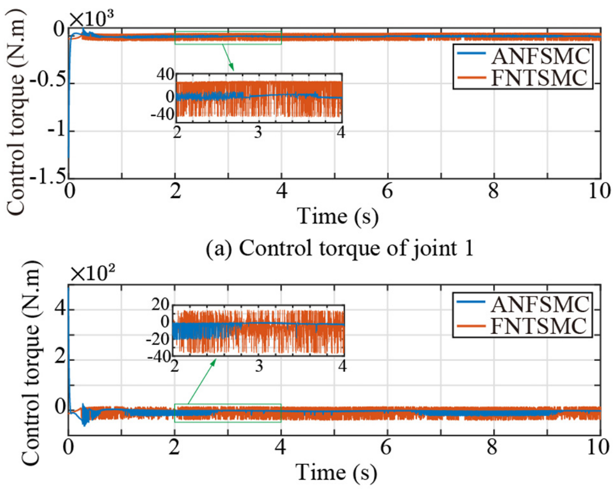

(a) Control torque of joint 1

(b) Control torque of joint 2

Fig. 17. ANFSMC and FNTSMC control torque.

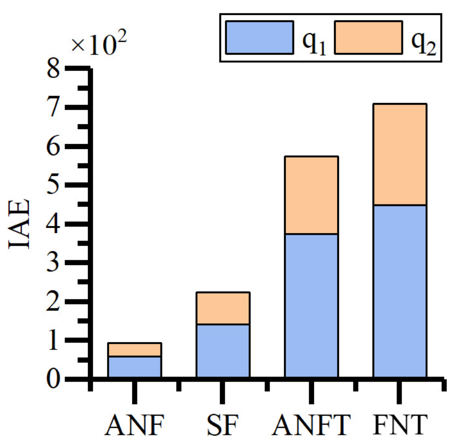

Fig. 18. Absolute tracking errors of controllers.

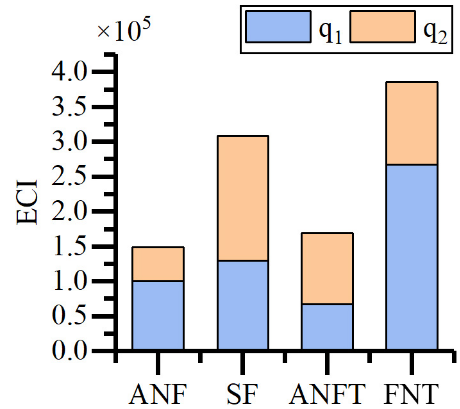

Fig. 19. Energy consumptions of controllers.

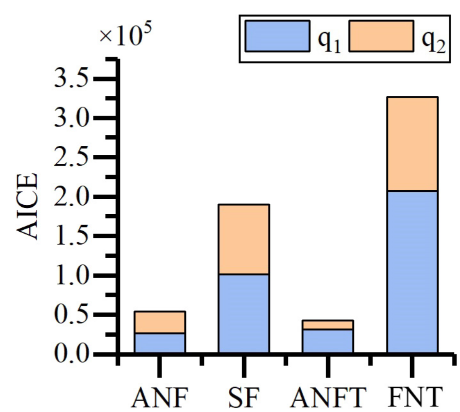

Fig. 20. Absolute control torque chattering error.

than the proposed controller, because the proposed controller requires a large control torque at the beginning of the robotic manipulator movement. Overall, the proposed ANFSMC scheme exhibits excellent performance in terms of trajectory tracking, energy consumption, and chatter suppression.

4.4. Performance evaluation of ANFSMC-AS

The performance of ANFSMC-AS is now described to illustrate the effectiveness of the proposed actuator saturation compensator in the ANFSMC scheme. The initial auxiliary variable ζ_0 is set to 0.006 and the saturation threshold value is [-50 50]. The ANFSMC controller without actuator saturation is also compared with the ANFSMC controller with consideration of actuator saturation but without compensation. The results are shown in Figs. 21–26.

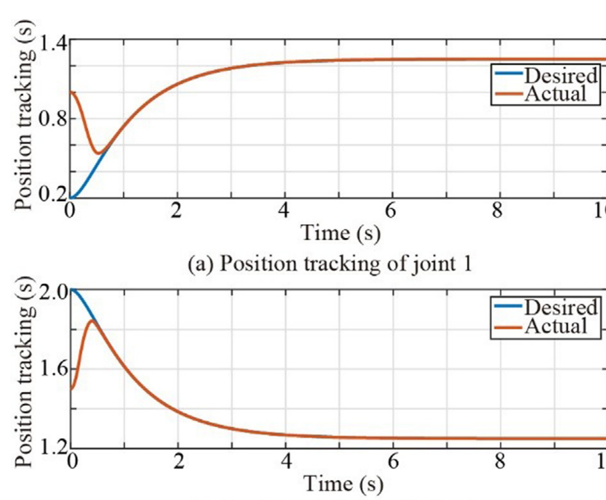

(a) Position tracking of joint 1

(a) Position tracking of joint 1

Fig. 21. Position tracking performance.

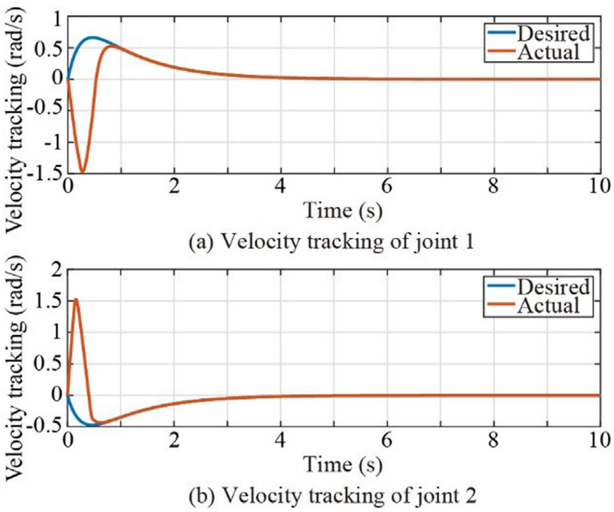

Fig. 22. Velocity tracking performance.

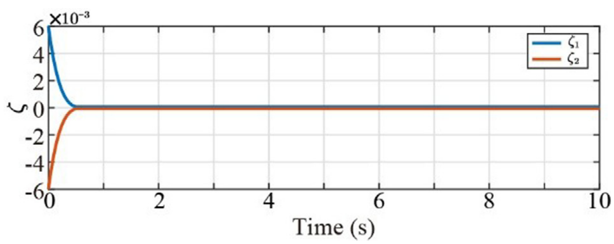

Fig. 23. Compensator parameter prediction.

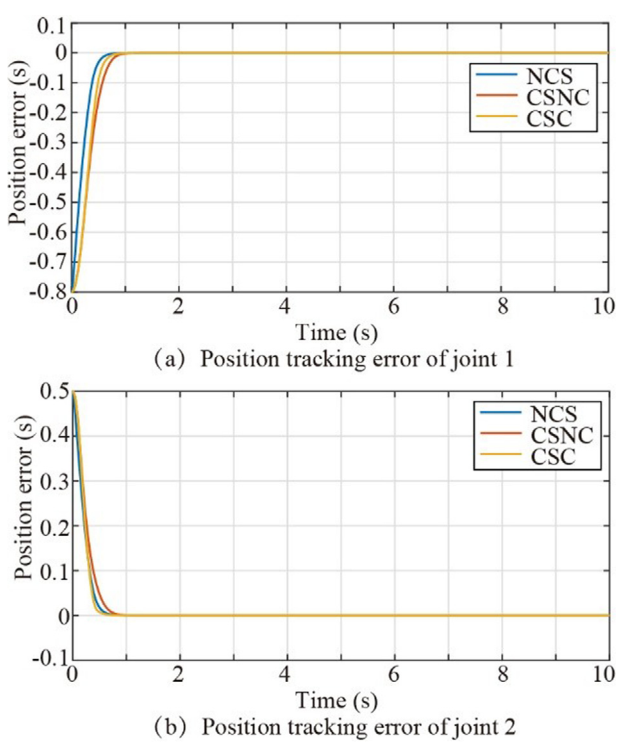

Fig. 24. Position tracking error performance.

Fig. 21 shows the position tracking performance and Fig. 22 shows the velocity tracking performance. In Fig. 23, the predicted value of the compensator parameter rapidly converges to a constant, indicating the strong compensation effect when the manipulator starts to track the ideal trajectory. From Fig. 24, it can be obtained that actuator saturation slows the convergence rate of the trajectory error in ANFSMC. Under the action of the compensator, the influence of actuator saturation can be eliminated and the convergence rate of the trajectory error can be accelerated. In Fig. 25, the control torque of the proposed ANFSMC-AS is smoother and the chattering is significantly alleviated. Finally, in Fig. 26, the AICE metric defined in Section 4.3 is used to compare the absolute control torque chattering error, where NCS represents the ANFSMC controller without considering actuator saturation, CSNC represents the ANFSMC controller considering actuator saturation but without compensation, and CSC represents the ANFSMC controller considering actuator saturation and compensation. It can obtain that the proposed compensator greatly alleviates the chattering of the system, leading to a reduction in AICE of 71.1%. Additionally, after considering the saturation compensation, the system chattering of the developed controller is much smaller than that in ANFTSMC.

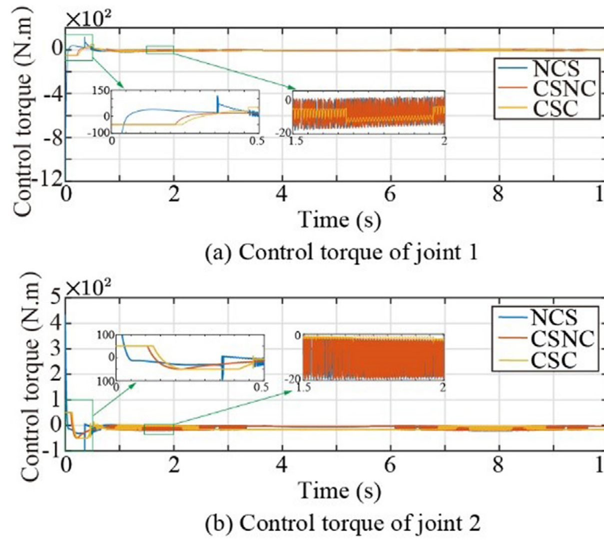

Fig. 25. Control torque of joints 1 and 2.

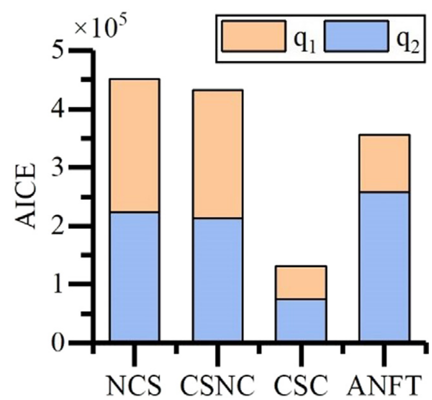

Fig. 26. Absolute control torque chattering error.

4.5. Discussion on comparison with existing methods

According to the above simulation, compared to the existing fixed-time and finite-time SMC schemes, the superiorities of the proposed controllers are highlighted as follows.

(1) Compared with the existing finite-time SMC scheme, as described FNTSMC [8] and ANFTSMC [29], the convergence time of the proposed controllers is independent of the initial states. In other words, we can estimate the settling time of the tracking errors of robotic manipulators without an initial position in advance. This feature makes the proposed control schemes suitable for robotic manipulators with error convergence time constraints. Moreover, faster convergence rate and higher tracking accuracy can be obtained compared with the other two methods.

(2) Compared with the existing fixed-time SMC scheme, as described SFSMC [19], the model or the exact upper bound of the disturbance is unnecessary in our proposed control scheme. This makes it easier to be applied to industrial robotic manipulators.

(3) According to the three evaluation indicators, including IAE, ECI, and AICE, the proposed control scheme has better performance in tracking precision, energy consumption, and chattering elimination. Moreover, the proposed controller saturation compensator can mitigate the adverse effects of actuator saturation due to the large initial control torque. This is always ignored in existing fixed-time SMC schemes for robotic manipulators.

5. Conclusion

This paper has described a new adaptive nonsingular fixed-time SMCer that considers the uncertainties of the robotic manipulator model and external disturbances, as well as actuator saturation. The proposed controller has the advantage of nonsingular fixed-time SMC, and fixed-time trajectory tracking of the manipulator can be realized without knowing the model or the exact upper bound of the disturbance. The saturation caused by excessive actuator torque is compensated by the actuator saturation compensator, allowing the chatter of control torque to be reduced by 71.1%, which makes the proposed control scheme highly suitable for practical industrial robotic manipulators. Comparisons between the proposed control scheme and other existing controllers in the case of a time-varying external disturbance proved that the proposed control scheme has a faster convergence rate, less control torque chattering, and greater robustness. In the future, the applications of the proposed scheme will be mainly focused on, and the smoother torque control schemes will also be studied.

CRediT authorship contribution statement

Huayang Sai: Conceptualization of this study, Methodology, Software. **Zhenbang Xu:** Assisted in perfecting the control scheme, Made important amendments to the paper. **Shuai He:** Assisted with data analysis. **Enyang Zhang:** Assisted with data analysis. **Lin Zhu:** Performed manuscript editing.

Declaration of competing interest

The authors declare that they have no known competing financial interests or personal relationships that could have appeared to influence the work reported in this paper.

References

[1] Yi S, Zhai J. Adaptive second-order fast nonsingular terminal sliding mode control for robotic manipulators. ISA Trans 2019;90:41–51.
[2] Wang Y, Zhu K, Chen B, Jin M. Model-free continuous nonsingular fast terminal sliding mode control for cable-driven manipulators. ISA Trans 2020;98:483–95.
[3] Jing C, Xu H, Niu X. Adaptive sliding mode disturbance rejection control with prescribed performance for robotic manipulators. ISA Trans 2019;91:41–51.
[4] Ahmed S, Wang H, Tian Y. Adaptive high-order terminal sliding mode control based on time delay estimation for the robotic manipulators with backlash hysteresis. IEEE Trans Syst Man Cybern: Syst 2019.
[5] Lau JY, Liang W, Tan KK. Adaptive sliding mode enhanced disturbance observer-based control of surgical device. ISA Trans 2019;90:178–88.
[6] Wu Y, Yu X, Man Z. Terminal sliding mode control design for uncertain dynamic systems. Systems Control Lett 1998;34(5):281–7.
[7] Feng Y, Yu X, Man Z. Non-singular terminal sliding mode control of rigid manipulators. Automatica 2002;38(12):2159–67.
[8] Yang L, Yang J. Nonsingular fast terminal sliding-mode control for nonlinear dynamical systems. Internat J Robust Nonlinear Control 2011;21(16):1865–79.
[9] Lu K, Xia Y. Adaptive attitude tracking control for rigid spacecraft with finite-time convergence. Automatica 2013;49(12):3591–9.
[10] Wang L, Song Z, Liu X, Li Z, Fernando T, Iu HH. Continuous finite-time integral sliding mode control for attitude stabilization. IEEE Trans Circuit Syst II: Express Briefs 2019.
[11] Polyakov A. Nonlinear feedback design for fixed-time stabilization of linear control systems. IEEE Trans Automat Control 2011;57(8):2106–10.
[12] Parsegv S, Polyakov A, Shcherbakov P. On fixed and finite time stability in sliding mode control. In: Proceedings of 4th IFAC workshop on distributed estimation and control in networked systems, Koblenz, Germany, 2013, p. 110–5.
[13] Polyakov A, Efimov D, Perruquetti W. Robust stabilization of MIMO systems in finite/fixed time. Internat J Robust Nonlinear Control 2016;26(1):69–90.
[14] Polyakov A, Efimov D, Perruquetti W. Finite-time and fixed-time stabilization: Implicit Lyapunov function approach. Automatica 2015;51:332–40.
[15] Cao L, Xiao B, Golestani M, Ran D. Faster fixed-time control of flexible spacecraft attitude stabilization. IEEE Trans Ind Inf 2019;16(2):1281–90.
[16] Golestani M, Esmailzadeh SM, Mobayen S. Fixed-time control for high-precision attitude stabilization of flexible spacecraft. Eur J Control 2020.
[17] Li H, Cai Y. On SFTSM control with fixed-time convergence. IET Control Theory Appl 2017;11(6):766–73.
[18] Zuo Z. Non-singular fixed-time terminal sliding mode control of non-linear systems. IET Control Theory Appl 2014;9(4):545–52.
[19] Zhang L, Wang Y, Hou Y, Li H. Fixed-time sliding mode control for uncertain robot manipulators. IEEE Access 2019;7:149750–63.
[20] Su Y, Zheng C, Mercorelli P. Robust approximate fixed-time tracking control for uncertain robot manipulators. Mech Syst Signal Process 2020;135:106379.
[21] Kumar N, et al. Finite time control scheme for robot manipulators using fast terminal sliding mode control and RBFNN. Int J Dynam Control 2019;7(2):758–66.
[22] Zhang D, Kong L, Zhang S, Li Q, Fu Q. Neural networks-based fixed-time control for a robot with uncertainties and input deadzone. Neurocomputing 2020.
[23] Chen Z, Yang X, Liu X. RBFNN-based nonsingular fast terminal sliding mode control for robotic manipulators including actuator dynamics. Neurocomputing 2019;362:72–82.
[24] Zhang Y, Hua C, Li K. Disturbance observer-based fixed-time prescribed performance tracking control for robotic manipulator. Internat J Systems Sci 2019;50(13):2437–48.
[25] Ajwad SA, Iqbal J, Khan AA, Mehmood A. Disturbance-observer-based robust control of a serial-link robotic manipulator using SMC and PBC techniques. Stud Inform Control 2015;24(4):401–8.
[26] Hu Q, Li B, Qi J. Disturbance observer based finite-time attitude control for rigid spacecraft under input saturation. Aerosp Sci Technol 2014;39:13–21.
[27] Yan W, Fei J. Adaptive control of MEMS gyroscope based on global terminal sliding mode controller. Math Probl Eng 2013;2013.
[28] Mondal S, Mahanta C. Adaptive second order terminal sliding mode controller for robotic manipulators. J Franklin Inst B 2014;351(4):2356–77.
[29] Boukattaya M, Mezghani N, Damak T. Adaptive nonsingular fast terminal sliding-mode control for the tracking problem of uncertain dynamical systems. ISA Trans 2018;77:1–19.
[30] Cao L, Xiao B, Golestani M. Robust fixed-time attitude stabilization control of flexible spacecraft with actuator uncertainty. Nonlinear Dynam 2020;1–15.
[31] Jiang B, Hu Q, Friswell MI. Fixed-time attitude control for rigid spacecraft with actuator saturation and faults. IEEE Trans Control Syst Technol 2016;24(5):1892–8.
[32] Lu K, Xia Y, Fu M. Controller design for rigid spacecraft attitude tracking with actuator saturation. Inform Sci 2013;220:343–66.
[33] Xiao B, Cao L, Xu S, Liu L. Robust tracking control of robot manipulators with actuator faults and joint velocity measurement uncertainty. IEEE-ASME Trans Mechatron 2020;25(3):1354–65.
[34] Jia S, Shan J. Finite-time trajectory tracking control of space manipulator under actuator saturation. IEEE Trans Ind Electron 2019;67(3):2086–96.
[35] Bhat SP, Bernstein DS. Finite-time stability of continuous autonomous systems. SIAM J Control Optim 2000;38(3):751–66.
[36] Khalil HK, Grizzle JW. Nonlinear systems, vol. 3. Prentice hall Upper Saddle River, NJ; 2002.
[37] Zuo Z, Tie L. Distributed robust finite-time nonlinear consensus protocols for multi-agent systems. Internat J Systems Sci 2016;47(6):1366–75.

[38] Zuo Z, Tie L. A new class of finite-time nonlinear consensus protocols for multi-agent systems. Internat J Control 2014;87(2):363–70.
[39] Spong MW, Hutchinson S, Vidyasagar M, et al. Robot modeling and control. 2006.
[40] Zhihong M, Palaniswami M. Robust tracking control for rigid robotic manipulators. IEEE Trans Automat Control 1994;39(1):154–9.
[41] Zhu W-H. Comments on ''robust tracking control for rigid robotic manipulators''. IEEE Trans Automat Control 2000;45(8):1577–80.

Sai Hua-Yang received a B.E. degree in School of Mechanical and Electronic Engineering form Northwest Agriculture and Forestry University, Yangling, China, in 2018. He is now a Ph.D. candidate in Mechanical Engineering and Automation, Changchun Institute of Optics, Fine Mechanics and Physics, Chinese Academy of Science, China. He is also currently pursuing the degree with the College of Optoelectronics, University of Chinese Academy of Sciences, Beijing. His current research interests include medical robot, robot robust control.

Xu Zhen-Bang received the B.E. degree from the Department of Theoretical and Applied Mechanics, Chinese Academy of Sciences University, Hefei, China, in 2005, and the Ph.D. degree from the Chinese Academy of Sciences University, in 2010, where he is currently with the Changchun Institute of Optics, Fine Mechanics and Physics. His research interests include space intelligent robot, multi-dimensional precision adjustment mechanism, space structure dynamics, and microvibration control.

He Shuai received a B.E.degree from University of Science and Technology of China, China, in 2011, and M.E. degree in University of Chinese Academy of Sciences, China, in 2014. His current research interests include mechanics analysis, kinematics, and dynamics of robots.

Zhang En-Yang received the B.E. degree from the Department of mechanical engineering and automation, Nanjing University of Aeronautics and Astronautics, Nanjing, China, in 2010, and the M.E. degree from Nanjing University of Aeronautics and Astronautics, in 2013, where he is currently with the Changchun Institute of Optics, Fine Mechanics and Physics. His research interests include space intelligent robot and space structure dynamics.

Zhu Lin received a bachelor's degree in physics form Northeast Normal University, Changchun, China, in 2018. She, a Ph.D. candidate, is mainly engaged in advanced optical imaging technology and space camera optical design research in optical engineering, Changchun Institute of Optics, Fine Mechanics and Physics, Chinese Academy of Science, Changchun, China and University of Chinese Academy of Sciences, Beijing.